DEFORMATION IN FOSSIL AND ACTIVE CONVERGENT TECTONIC REGIONS

DEFORMATION IN FOSSIL AND ACTIVE CONVERGENT TECTONIC REGIONS: EXAMPLES FROM SUDBURY, ONTARIO, AND RHODES, GREECE

By Martin D. Clark, B.Sc.

A Thesis Submitted to the School of Graduate Studies in Partial Fulfillment of the Requirements for the Degree Master of Science

McMaster University MASTER OF SCIENCE (2012) Hamilton, Ontario (Earth Science)

TITLE: Deformation in fossil and active convergent tectonic regions: examples from Sudbury, Ontario, and Rhodes, Greece AUTHOR: Martin D. Clark, B.Sc. (McMaster University) SUPERVISOR: Professor U.P. Riller NUMBER OF PAGES: xi, 65

Abstract

The kinematics and associated deformation of upper crust in fossil and active convergent tectonic settings require different methods of study. In this thesis, I analyzed an example of a fossil convergent setting, the formation of the eastern portion of Paleoproterozoic Sudbury Basin, Ontario, and an example of an active convergent plate interface represented by the ongoing subduction along the Hellenic Arc at Rhodes, Greece. In Sudbury, using paleomagnetic remanence directions and Matachewan dyke orientations, I constrain the magnitudes of rotation associated with the formation of the NE-lobe, a tight secondary fold of the Sudbury Basin, as well as localize the fold axis and magnitude of rotation along the West Bay Anticline, a hitherto unknown fold of the Basin.

For the Island of Rhodes, I corroborate the existence of two phases of Plio-Pleistocene or younger deformation including providing their principal strain axis orientations from a fault-slip analysis. In addition, I estimate the magnitude of slip from faults to generate respective incremental strain ellipses of the two deformation phases for the Island. The first phase is characterized by vertical shortening ($\hat{s}_3$) and N-S extension ($\hat{s}_1$) with associated normal faulting while the second phase is characterized by N-S shortening ($\hat{s}_3$) and E-W extension ($\hat{s}_1$) associated with strike-slip faulting.

Acknowledgements

The order in which I present my acknowledgements have no bearing on the importance of each person.

First, I'd like to give my indebted thanks to Dr. Bill Morris, Dr. Joe Boyce, and Mr. Pat Deluca for their instruction through my undergraduate degree. The way I approached and conducted this study is based on the various teachings I received. Dr. Morris's paleomagnetic expertise along with his extensive knowledge of the Sudbury area helped greatly in understanding the data and various processes of Sudbury related deformation. Seminars with Dr. Boyce's provided new insights to methods of extracting slip orientations and magnitudes along with his knowledge of tectonics of the Aegean-Anatolian area were always helpful and ensured a level of quality and consistency in the results. Mr. Deluca helped me cultivate my current understanding of scientific analysis within a G.I.S. and was always able to provide help, notably with the specifics of kriging interpolation routines. Acting as a teaching assistant for Mr. Deluca also helped me develop how to convey material regardless of its topic.

Second, I'm very grateful for the time, company, and help I've received from everyone who was a part of the structural kinematics lab, namely: Heidi Daxberger, Iris Lenauer, Lucie Mathieu, Laura Wright, and Tasca Santimano. The discussions of fault slip analysis and surficial processes with Heidi were invaluable to the completion of this study. Moreover, discussions with Iris aided to better understand characteristics of the Sudbury Basin vital to the results presented. Lucie Mathieu influenced the manner I present this study, acting always to help ensure the high level of quality of scientific analyses. Laura Wright helped me stay focused, through various discussions of the advances and drawbacks of the analyses. Lastly, Tasca Santimano helped my academic and professional development from being a great coworker in the mining sector to being a part of our study team in Thode Library. These times always helped me stay on track, focused, and content with the status of my work.

Third, I'd like to provide thanks to everyone in the center for spatial analysis for their help with my analysis, most notably Matthew Adams for help with Python coding.

Forth, I'd like to thank Dr. Bruce Jago and Dr. Alar Soever along with everyone at Wallbridge Mining Company for their help in my data collection and education of Sudbury geology and associated processes.

Fifth, I should thank my friends and family for the support since the beginning.

Lastly, I must thank my supervisor Dr. Ulrich Riller. Outside of his profound contribution to my academic, professional, and personal development, the most important thing I learned was to keep going regardless of my reservations. He helped me develop in many ways from providing academic opportunities such as my attendance to international conferences, to guiding me through the scientific publication process. I'm very grateful for the manner in which he has guided my studies.

Thank you all for your help.

Table of Contents

Lists of Figures and Tables

List of all Abbreviations and Symbols

σ – Stress

ŝ – Strain

° – Degree

Declaration of Academic Achievement

All research presented was conducted and synthesized by Martin D. Clark. Dr. Ulrich Riller helped editing all chapters and Dr. Bill Morris edited parts of Chapter 2. A python script to help extract the horizontal component of slip vectors was written by Matthew Adams.

Chapter 1 – Introduction

The methods used by scientists to study active and fossil convergent tectonic settings differ greatly. Active convergent tectonic settings generally have many indicators of deformation which include actively deforming rocks with associated geomorphic responses (i.e., earthquakes, landslides, and subsidence/uplift of surfaces) allowing for use of active monitoring systems such as global positioning system (GPS) tracking of plate movements, seismology of ongoing tectonic activity, surficial geophysical surveys, and active mapping. Fossil convergent tectonic settings can be a challenging topic as they are restricted in the types of deformation indicators available as subsequent geological processes can modify, destroy, or hide important features. Therefore, display proxies of deformation due to erosion of features and accumulated sedimentary cover since its activity. Methods of study include analysis of deformation markers, drilling and subsequent subsurface 3D mapping, and subsurface geophysical surveys.

Here, I present an analysis of upper-crustal deformation associated with fossil and active collisional tectonic settings using two locations: The Sudbury Basin, Ontario, and the Island of Rhodes, Greece. A variety of methods are employed to study deformation in fossil collisional tectonic settings including an analysis of markers such as paleomagnetic vectors and dyke swarm orientations. For active collisional tectonic settings, an analysis of Pliocene to active faults is conducted followed by a fault-slip analysis and a calculation of sectional strain ellipses.

Chapter 2 – Upper-crustal, basement-involved folding in the East Range of the Sudbury Basin, Ontario, inferred from paleomagnetic analysis and spatial analysis of mafic dykes

2.1. Introduction

Understanding mechanisms of non-cylindrical, basement-involved folding on the regional scale remains a challenging topic to structural analysts studying deformed basement terranes (e.g., Erslev 1986; Kley et al. 1996; Cristallini et al. 1997; Chen 1998). Particularly in cases where such deformation occurred close to the Earth's surface, folding strain in crystalline rocks is not easily recognized. More specifically, the extent and scale at which strain fabrics are associated with folding-induced shape change of basement rocks is difficult to assess (Choukroune and Gapais 1983; Gapais et al. 1987). Participation of crystalline basement rocks in large-scale folding is commonly identified by the presence of a folded interface with sedimentary cover rocks. However, such marker horizons as well as those within crystalline rocks are not always present. In cases where they are, there is often uncertainty about their pre-deformational configuration. Collectively, these structural circumstances hamper an appraisal of rotational deformation components particularly in weakly- or non-layered basement rocks. Paleomagnetic fold tests can help constrain rotational components in such rocks, but their successful application requires knowledge of specific fold elements, notably the position of the hinge line and the spatial extent of fold limbs.

The Sudbury Basin (Fig. 1) is an excellent target to study the participation of crystalline rocks in folding strain at uppermost crustal levels. This is because the perimeter of this non-cylindrical and asymmetric fold basin is made up of igneous rocks produced by a layered impact melt sheet, the Main Mass of the Sudbury Igneous Complex, herein referred to as SIC (Fig. 1). In the north and east, the SIC is underlain by

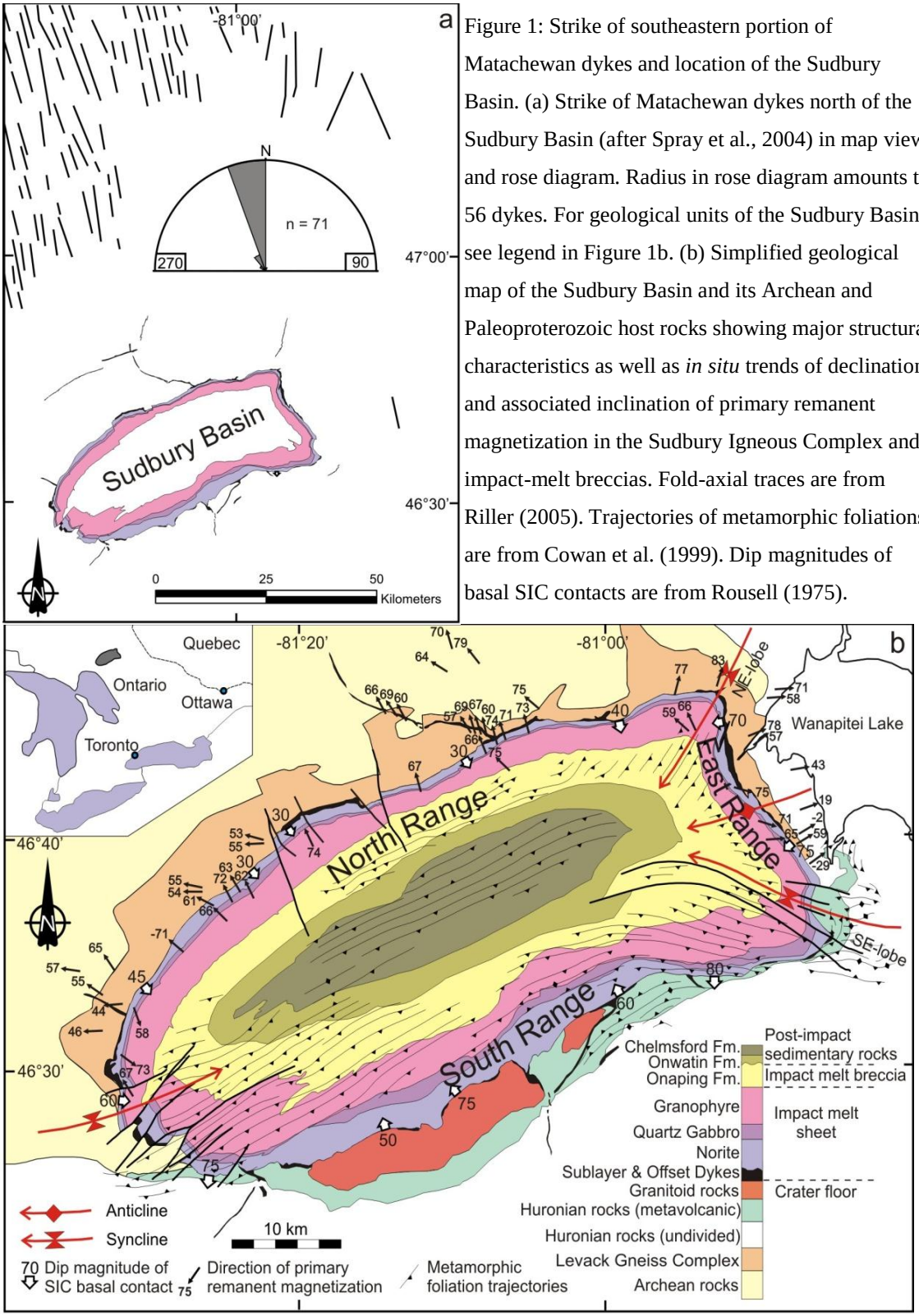

Figure 1: Strike of southeastern portion of Matachewan dykes and location of the Sudbury Basin. (a) Strike of Matachewan dykes north of the Sudbury Basin (after Spray et al., 2004) in map view and rose diagram. Radius in rose diagram amounts to 56 dykes. For geological units of the Sudbury Basin see legend in Figure 1b. (b) Simplified geological map of the Sudbury Basin and its Archean and Paleoproterozoic host rocks showing major structural characteristics as well as *in situ* trends of declination and associated inclination of primary remanent magnetization in the Sudbury Igneous Complex and impact-melt breccias. Fold-axial traces are from Riller (2005). Trajectories of metamorphic foliations are from Cowan et al. (1999). Dip magnitudes of basal SIC contacts are from Rousell (1975).

Archean crystalline basement rocks (Fig. 1b). Strain in the northeastern SIC and its basement rocks during folding accumulated mostly by brittle deformation (Klimczak et al. 2007). The interface between the two crystalline rock masses is devoid of any contact strain (Dressler 1984). Collectively, these structural characteristics indicate that the SIC and Archean basement rocks behaved mechanically the same during folding. The magnitude of tilting of the SIC and identification of secondary fold structures that extend into basement rocks (Fig. 1b) can be inferred from the orientation of SIC contacts (Rousell 1975; Dreuse et al. 2010). Moreover, mafic dykes in Archean basement rocks underlying the East Range SIC (Fig. 2) were emplaced prior to folding and can be used as markers to constrain domains that underwent similar rotations in basement rocks.

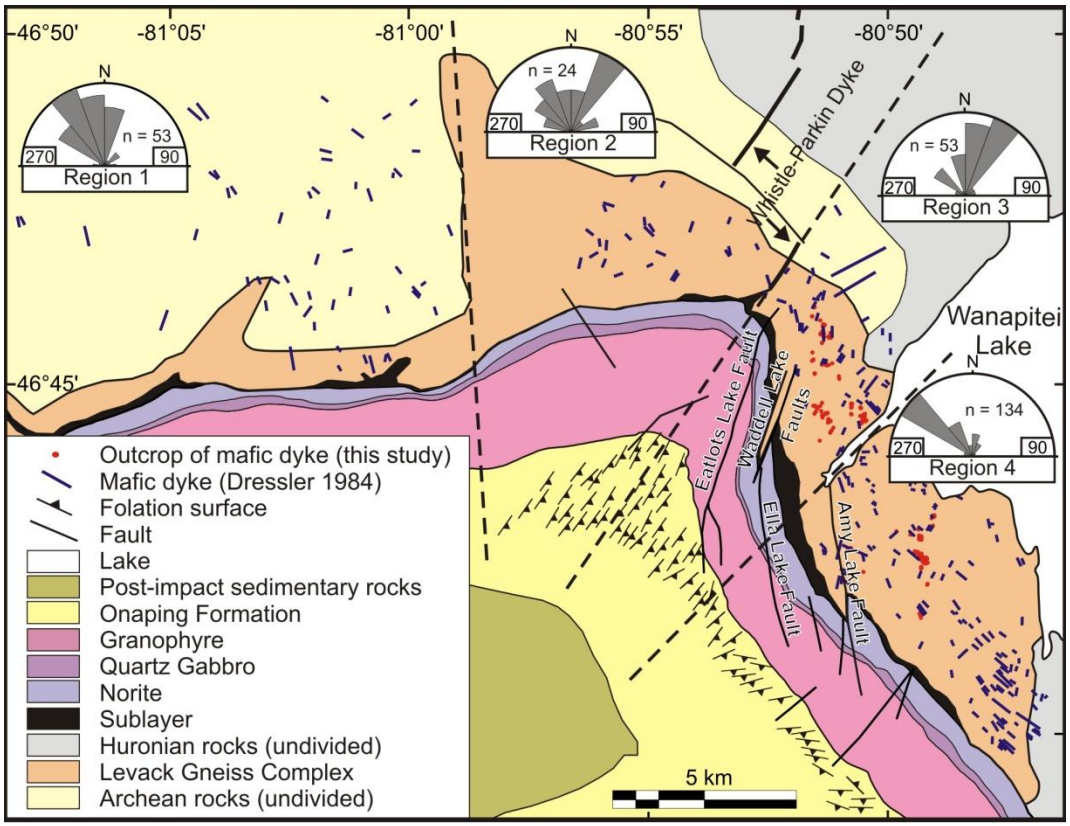

Figure 2: Geological map of the northeastern Sudbury Basin and adjacent Archean basement rocks showing the distribution of mafic dykes after Dressler (1984) and the location of dyke occurrences from this study. Foliation orientations in the Onaping Formation are from Cowan (1999). Rose diagrams show the dyke strikes for regions 1 to 4, the boundaries of which are indicated by stippled lines. Radii of rose diagrams for regions 1 to 4 are respectively 14, 6, 16 and 59 dykes.

Due to the structural complexity and potential for Cu-Ni-sulfide deposits associated with the base of the SIC (Keays and Lightfoot 2004), the eastern Sudbury Basin is of particular interest in resolving how folding strain accumulated in these crystalline rocks. The eastern Basin contains two higher-order synclines, the NE-lobe and the SE-lobe, and an apparently west-plunging anticline between the synclines (Riller 2005). The lobes divide the SIC into weakly curved segments that are topographically elevated and known as the North Range, the East Range and the South Range (Fig. 1b). Structural uncertainties associated with the East Range include the mechanisms that produced the steeply dipping basal contact of the SIC and the localization of higher-order lobes, the fold-axial traces of which are at a high angle to each other (Fig. 1b). The location and orientation of the fold-axial trace of the anticline is not well constrained. South of the NE-lobe, the SIC is displaced by three major fault zones, the Eatlots Lake Fault, the Waddell Lake Faults and the Amy Lake Fault (Fig. 2). These faults and the Ella Lake Fault, located south of the Waddell Lake Faults, are curved and characterized by sinistral strike separations of SIC contacts. The genesis of the curvature of these faults and whether they are related to folding of the SIC is uncertain. Finally, it is unknown to what extent and how Archean basement rocks participated in folding of the SIC.

I address basement-involved folding of the eastern Sudbury Basin by reassessing published paleomagnetic data from the North Range and the East Range to identify tilt magnitudes of the limbs of the NE-lobe. In contrast to previous paleomagnetic studies reporting rotations around horizontal axes that are parallel to the strike of the SIC in both Ranges (Morris 1984; Szabó and Halls 2006; Halls 2009), I use the hinge line orientation of the NE-lobe as indicated by structural data (Klimczak et al. 2007) to infer tilt magnitudes of the SIC. I analyze the spatial distribution of strike directions of mafic dykes in Archean rocks (Dressler 1984) to identify coherent rotation domains in the Archean basement rocks and correlate these with paleomagnetic rotations. Finally, I constrain the location of the fold-axial trace of the anticline and provide explanations for

the localization of the NE-lobe as well as for the kinematics and curvature of major fault zones in the East Range.

2.2. Geological background information

The Sudbury Basin (Fig. 1) occupies the central portion of the Sudbury Impact Structure, estimated to be > 150 km in diameter (Grieve et al. 1991; Deutsch et al. 1995; Spray et al. 2004, Pope et al. 2004; Grieve et al. 2008). The Basin is made up of the 1.85 Ga SIC (Krogh et al. 1984), melt breccias of the Onaping Formation (Grieve et al. 2010) and post-impact clastic sedimentary rocks of the Whitewater Group (Fig. 1b). To the north and east, the SIC overlies metagranitoid rock, gneiss and migmatite of the ca. 2.7 Ga Levack Gneiss Complex (Figs. 1b, 2). To the south, the basal SIC is in contact with ca. 2.45 Ga metavolcanic rocks of the Paleoproterozoic Huronian Supergroup and ca. 2.3 Ga granitoid plutons (Fig. 1). Emplacement of the SIC resulted in a ca. 1-2 km wide contact metamorphic aureole and partial melting in Archean and Paleoproterozoic host rocks (Dressler 1984; Riller et al. 1996; Boast and Spray 2006; Pentek et al. 2011). However, there is no evidence of contact metamorphism in the overlying Onaping Formation (Grieve et al. 2010).

Because of its synformal geometry and layering, the SIC was interpreted initially as a laccolith (Coleman 1907) or lopolith (Wilson 1956). Recognition of shock-metamorphic structures in the Sudbury area (Dietz 1964; French 1968) led to a profound paradigm shift in the interpretation of melt rocks and breccias in the Sudbury area (Grieve et al. 1991; Deutsch et al. 1995). Most importantly, this led to a change in the interpretation of the SIC from an endogenic intrusion to a melt body generated by hypervelocity meteorite impact.

Based largely on the apparent lack of evidence for pervasive deformation in the NE-lobe, Cowan (1999) and Cowan et al. (1999) suggested that the SIC was emplaced as

a curvi-planar melt sheet into a pre-existing fold basin. However, a growing body of evidence indicates that the SIC formed as an impact melt sheet that was ponded in an impact crater with subhorizontal floor. Evidence includes (1) formation of the SIC by melting of its immediate host rocks (Grieve et al. 1991; Dickin et al. 1999; Therriault et al. 2002; Zieg and Marsh 2005), (2) lack of intrusive roof rocks of the SIC (Grieve et al. 2010), (3) gravity-driven chemical differentiation or separation of the SIC into petrographically distinct layers (Grieve et al. 1991; Dickin et al. 1999; Therriault et al. 2002; Zieg and Marsh 2005) and (4) estimates of thickness variations of the SIC constraining the variation in crater-floor topography (Dreuse et al., 2010). As a consequence, a fold origin for the Sudbury Basin is now widely accepted and is supported by the geometry of post-impact deformation structures, notably foliation surfaces that are axial-planar to the NE- and SW-lobes (Cowan and Schwerdtner 1994; Riller et al. 1998; Klimczak et al. 2007), shortening directions inferred from brittle faults (Cowan et al. 1999; Riller 2005; Klimczak et al. 2007) and paleomagnetic evidence (Morris 1984; Szabó and Halls 2006; Halls 2009).

The SIC consists of petrographically distinct layers, known from bottom to top as the Norite, Quartz Gabbro and Granophyre (Grieve et al. 1991). Breccia fragments in a noritic matrix form a discontinuous layer, the so-called Sublayer (Pattison 1979), at the base of the Norite (Fig. 1b). Quartz diorite dykes, known as Offset Dykes (Grant and Bite 1984), emanate from trough-shaped Sublayer embayments in Archean and Paleoproterozoic host rocks (Morrison 1984) and protrude sub-radially into these host rocks (Fig. 1). The embayments may have formed by thermal corrosion of host rocks imparted by superheated impact melt at the intersection of Offset Dykes and the impact melt sheet (Riller 2005; Hecht et al. 2008).

The basal contact of the SIC dips mostly towards the Basin center (Fig. 1), but dip magnitudes vary greatly with position (Rousell 1984; Dreuse et al. 2010). The North Range SIC forms a broad arc and shows little evidence of pervasive deformation (Cowan

1999). Here, the base of the SIC dips moderately toward the south (Fig. 1b). By contrast, the South Range SIC is strongly affected by deformation at the grain to meter scale due to reverse shearing on the South Range Shear Zone (Shanks and Schwerdtner 1991) and overall NW-SE shortening (Lenauer and Riller 2012). The base of the South Range SIC dips steeply toward the north and is overturned at the SE-lobe (Fig. 1). The East Range SIC dips steeply toward the west, but shows little evidence of pervasive deformation, despite its strong plan-view curvature, notably in the lobes (Cowan 1999; Klimczak et al. 2007).

Evidence for the fold origin of the NE-lobe, the fold hinge of which coincides spatially with the Whistle embayment and the Whistle-Parkin Offset Dyke (Fig. 2), is based on the orientation of SIC contacts (Fig. 1b) and of metamorphic foliation surfaces in the Onaping Formation (Cowan 1999). These foliation surfaces are concordant with the axial surface of the NE-lobe (Klimczak et al. 2007). The SIC is devoid of equivalent mineral fabrics in the NE-lobe suggesting that the SIC-Onaping Formation contact constitutes a major mechanical interface. However, planar magnetic fabrics in the Granophyre are concordant to the metamorphic foliation in the overlying Onaping Formation of the East Range (Cowan 1999). The magnetic fabrics in the Granophyre may, therefore, represent a weakly developed metamorphic fabric.

Klimczak et al. (2007) showed that large parts of the SIC in the NE-lobe were affected by brittle deformation on the grain scale and kilometer-scale deformation zones. Shortening directions inferred from slip senses on prominent NE-striking faults in the NE-lobe are orthogonal to the axial-planar foliation surfaces in the Onaping Formation (Klimczak et al. 2007). These structural relationships indicate that folding of the SIC in the NE-lobe, and most likely in the East Range, was accomplished by brittle deformation, which largely retained the map-view continuity of the SIC. It is noteworthy that internal SIC contacts are gradational and, like the SIC base, devoid of any contact strain. This

corroborates the notion that the Archean basement rocks behaved mechanically similar to the SIC during folding.

Four swarms of mafic dykes are known to occur in Archean rocks north and east of the Sudbury Basin: 2.45 Ga Matachewan dykes (Ernst and Halls 1984, Heaman 1997, Phinney and Halls 2001), 2.2 Ga Nipissing dykes (Corfu and Andrews 1986, Lightfoot et al. 1993), 2.17 Ga Biscotasing dykes (Buchan et al. 1993) and 1.23 Ga Sudbury dykes (Krogh et al. 1987, Dudas et al. 1994, Shellnutt and MacRae 2012). Matachewan diabase dykes strike mostly N-S north of the Sudbury Basin (Fig. 1a) and are recognized by up to several centimeter long phenocrysts of Ca-rich plagioclase set in a medium-grained matrix of intergrown plagioclase and clinopyroxene. Nipissing intrusions occur mostly as up to hundreds of meters wide irregular shaped gabbroic sills in Huronian rocks (Lightfoot et al. 1993). The sills are chiefly made up of coarse-grained orthopyroxene, clinopyroxene and some plagioclase and do not show a preferred orientation. Biscotasing dykes strike generally NE-SW to ENE-WSW (Buchan et al. 1993). Except for the presence of prominent plagioclase phenocrysts, their mineralogical composition is similar to that of Matachewan dykes. Dykes of the Sudbury swarm are highly magnetic, strike uniformly NW-SE to WNW-ESE, transect tilted portions of the SIC, and are easily identified by their light brown weathering color caused by the high content in olivine.

2.3. Previous paleomagnetic studies

Hood (1961), Sopher (1963) and Larochelle (1969) noted a difference of up to 40° in paleomagnetic remanence directions between the North Range SIC and the South Range SIC, and thus provided the first evidence for post-emplacement tilting of the SIC. In subsequent paleomagnetic studies, remanence directions of the SIC were separated into directions of primary remanent magnetization, acquired upon cooling of the SIC, and secondary magnetization directions due to metamorphism or hydrothermal alteration (Morris 1980a, 1980b, 1981, 1982, 1984). Morris (1984) also recognized that primary

remanence directions in the North Range SIC are orthogonal to the strike of the SIC (Fig. 1b), corroborating post-emplacement rotation of the SIC.

In order to identify the orientation of the remanent magnetization vector for the SIC prior to tilting, Morris (1980b) rotated the paleomagnetic vectors of the North Range and the East Range around horizontal axes that are parallel to the local trends of the respective Ranges. The South Range was excluded from this exercise as almost all remanence directions there were found to be secondary. Morris (1980b) obtained a mean paleomagnetic remanence direction of 199/88 for the SIC by rotating the western North Range, the eastern North Range and the East Range by respectively 42°- 47°, 24° and 61°. This resulted in a pre-tectonic configuration of the SIC in which the western North Range SIC is horizontal, the eastern North Range SIC dips 20° S and the East Range SIC dips 14° SW.

Paleomagnetic rotations based on remanence vectors from the SIC leave open the extent to which Archean host rocks participated in post-impact tilting of the North Range and the East Range. Therefore, Szabó and Halls (2006) used paleomagnetic remanence directions obtained from impact melt breccias in Archean basement rocks underlying the North Range and the East Range. Back rotation of the North Range and the East Range again around horizontal axes resulted in a mean remanence orientation of 199/79. Specifically, this orientation was achieved by rotating the western North Range, the eastern North Range and the East Range by respectively 36°, 22° and 36°. These rotations resulted in a pre-tectonic dip of the western North Range, the eastern North Range and the East Range of respectively of 0-9° S, 18° S and 34° W.

In summary, the studies by Morris (1980b) and Szabó and Halls (2006) resulted in a nearly identical mean paleomagnetic remanence orientation for the SIC and similar rotation magnitudes for the North Range. However, none of the studies resulted in an initially subhorizontal base of the SIC. In fact, paleomagnetic rotations are consistently

lower than the respective dips of the basal SIC contact in the North Range and the East Range (Fig. 1b). The largest departure in the inferred pre-tectonic orientation between the SIC and underlying Archean rocks is observed for the East Range. This discrepancy in rotation magnitude may be due to complex deformation and, hence, differential rotation of rocks within the East Range and Archean rocks. Alternatively, the assumption that the rocks should be rotated around horizontal axes may not be valid.

2.4. Methods

Paleomagnetic data from rocks of the SIC or from matrices of impact-generated pseudotachylite bodies was compiled from published sources (Morris 1980a, 1980b, 1981, 1982; Morris and Pay 1981; Szabó and Halls 2006) and separated into directions of primary and secondary remanence directions. Primary remanence directions used for paleomagnetic rotations of the North and East Range SIC are, therefore, 1.85 Ga in age (Table 1). The locations of the remanence directions (Fig. 1) were obtained either from the respective coordinates indicated in the published sources or, in cases in which no coordinates were provided, by georeferencing of location maps in the published sources. Remanence directions from the SIC and pseudotachylite bodies in Archean rocks that were deformed during formation of the NE-lobe were geometrically averaged after Fisher (1953) and rotated around the lobe's fold axis (197/35: plunge direction/plunge) inferred from structural field data (Klimczak et al. 2007). I assumed that both limbs of the NE-lobe rotated by the same magnitudes (Fig. 3).

Table 1: Compiled primary remanence values from paleomagnetic studies of the Sudbury Basin.

Sample ID	Easting (NAD27)	Northing (NAD27)	Lithology[a]	N[b]	D (°)[c]	I (°)[d]	k[e]	α95[f]	Source
1	516219.3	5167784	BX	7	59.7	58.7	52	8.4	[1]
2	517253.6	5166260	BX	5	56.6	-28.8	39.4	12.3	[1]
3	516425.7	5168591	BX	7	60.3	-1.6	12	18.5	[1]
4	516513.8	5170393	BX	4	70.6	18.6	62.5	11.7	[1]
5	515788.2	5173466	BX	5	80.1	43	341.8	4.1	[1]
7	512193.0	5175741	BX	7	69.9	78	23.7	13.7	[1]
8	512586.7	5175738	BX	4	52.4	57.2	147.8	7.6	[1]
9	513759.4	5179101	BX	5	84.8	57.5	14.6	20.7	[1]
10	514406.1	5179776	BX	7	85.6	71.1	80	6.8	[1]
13	509147.3	5180529	BX	4	18.8	83	52.7	12.8	[1]
15	505629.0	5179852	BX	3	15.7	77.4	90.2	13.1	[1]
16	493636.4	5178512	BX	6	310.3	74.7	53.5	9.2	[1]
17	488509.1	5182274	BX	5	318.6	79.3	54	10.5	[1]
18	485662.6	5181452	BX	5	301	63.6	78.8	8.7	[1]
19	486468.1	5183507	BX	5	343.4	70.1	32.2	13.7	[1]
20	470528.8	5167560	BX	13	283.4	53.3	15.4	10.9	[1]
21	470528.8	5167560	BX	4	268	54.7	38.4	15	[1]
22	455270.5	5157136	BX	3	279	57.2	80.7	13.8	[1]
23	457173.4	5155553	BX	6	305.4	54.7	36.5	11.2	[1]
24	458959.4	5154415	BX	8	264.9	44.9	70.6	6.6	[1]
25	457181.6	5152274	BX	4	267.8	46.2	46	13.7	[1]
26	458465.2	5157580	BX	7	325.8	65.1	39.8	9.7	[1]
27	466512.2	5162562	IN	7	295.8	60.6	279.4	3.6	[1]
28	465455.0	5163428	LG	3	282.2	55.1	223.2	8.3	[1]
29	465455.0	5163428	MD	3	282.4	54.4	87.2	13.3	[1]
30	465455.0	5163428	BX	3	271.9	54.4	84.2	13.5	[1]
35	459800.5	5147189	MP	7	327	67	311	3	[2]
40	459903.9	5150011	MP	9	125	73	109	5	[2]
42	460677.8	5153389	MP	6	162	58	119	6	[2]
43	464026.7	5159031	OD	4	309	-71	39	15	[3]
45	467701.0	5161537	MP	7	312	66	79	7	[2]
46	468327.5	5163097	MP	7	331	72	36	10	[2]
49	468970.2	5163883	MP	8	329	63	176	4	[2]
52	470110.9	5163473	MP	9	334	62	92	5	[2]
60	475051.8	5167655	MP	7	334	74	190	4	[2]
68	484128.6	5172048	MP	10	344	67	71	6	[2]
72	489947.3	5175434	MP	3	337	66	23	26	[2]
74	491235.4	5173593	MP	9	313	75	73	6	[2]

77	493139.1	5176757	MP	4	344	73	204	7	[2]
86	506180.0	5176790	MP	7	311	59	320	3	[2]
88	506933.5	5177028	MP	3	335	66	73	15	[2]
92	511032.7	5171778	MP	7	106	75	175	5	[2]
98	513070.9	5169104	MP	10	107	71	59	6	[2]
100	513735.1	5167858	MP	6	87	65	38	11	[2]
103	486945.8	5151287	MP	7	215	78	114	6	[2]
104	487290.5	5150151	MP	4	194	78	66	12	[2]
111	481733.9	5178102	OD	13	331	60	191	3	[3]
112	481733.9	5178102	OD	5	330	66	1113	2	[3]
113	481896.0	5178042	OD	6	331	69	207	6	[3]
116	482030.9	5177990	OD	5	322	62	79	9	[3]
127	488958.3	5176647	OD	3	342	69	44	19	[3]
130	489473.2	5176633	OD	9	343	57	60	7	[3]
135	489473.2	5176633	OD	7	324	67	71	7	[3]
138	489473.2	5176633	OD	5	342	60	207	5	[3]
150	490327.9	5175947	OD	11	341	71	109	4	[3]
152	489977.9	5175702	OD	5	345	74	48	11	[3]
193	465966.6	5178817	DI	7	346	56	55	8	[4]

[a]BX: Sudbury Breccia, DI: Diabase, IN: Intermediate Norite MD: Matachewan Diabase, MP: Micropegmatite LG: Levack Gneiss, OD: Offset Dyke

[b] Number of Samples

[c] Declination

[d] Inclination

[e,f] Fisher Precision Parameters

[1] Szabó and Halls 2006

[2] Morris 1981a

[3] Morris 1982

[4] Morris & Pay 1981

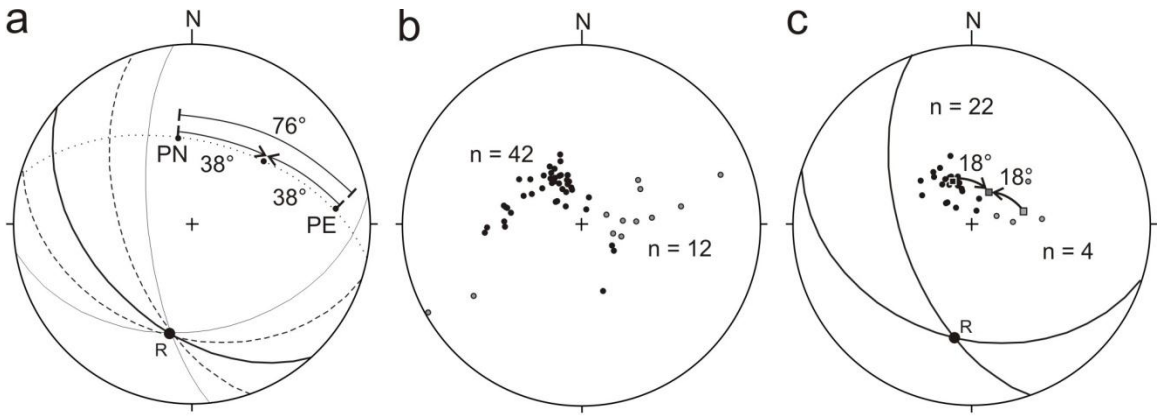

Figure 3: Lower-hemisphere equal-area projections showing orientations of basal SIC contacts, primary remanence directions and inferred unfolding magnitudes for the NE-lobe. (a) Unfolding of the North Range and East Range basal SIC contacts (solid great circles) and their respective poles, PN and PE, around the hinge line (R: 197/35) of the NE-lobe to a common plane (bold great circle). Limb rotations (38°) amount to a total unfolding magnitude of the NE-lobe (76°). Stippled great circles indicate partially unfolded SIC contacts, i.e., the orientations of contacts at the time of primary remanence acquisition. Dotted great circle demarcates the profile plane of the fold. (b) Orientations of primary remanent magnetization vectors of the North Range (black circles) and East Range (grey circles). (c) Unfolding magnitudes (18°) of the mean orientations (squares) of primary remanence directions of the eastern North Range (black circles) and northern East Range (grey circles) around the hinge line (R: 197/35) of the NE-lobe. Great circles indicate the orientations of North Range and East Range basal SIC contacts after unfolding.

Due to the outcrop conditions, neither my mapping of dykes nor that conducted by others, notably Dressler (1982) and Dressler (1984), resulted in reliable dip angles of dyke walls. Therefore, my spatial analysis is restricted to the strike directions of mafic dykes or dyke segments (Fig. 2). The analysis is based on the fact that mafic dykes of the Matachewan swarm strike approximately N-S in undeformed terranes just north of the Sudbury Basin (Ernst and Halls 1984, West and Ernst 1991). East of the Sudbury Basin, mafic dykes deviate in part significantly from this strike (Dressler 1982, 1984). The dyke data by Dressler (1982, 1984) was converted into GIS format by Ames et al. (2005) and this format was used in my analysis.

Because of the spatial heterogeneity of dyke segments, notably in terms of strike direction and non-uniform spacing between dyke segments, a kriging interpolation method was applied (Fig. 4). The interpolated surfaces were generated with the software *MapInfo Discover* using an ordinary kriging routine with a cell size of 50m, a search radius with its major axis oriented at 315° and a search distance of 1000m in both the major and minor directions. A variogram analysis indicates that a spherical model directed at 335° with a range of 925.3m, a nugget of 667.5m and sill of 876.5m best represent the dyke data (Fig. 5). To achieve the grid-coverage displayed in Figure 4, one search expansion and one grid pass was used. The kriging interpolation resulted in surfaces displaying dyke strikes ranging in azimuth from 270° to 90° (Fig. 4). These surfaces were used to identify the location of prominent rotation axes and structural discontinuities.

2.5. Results

Paleomagnetic rotations

Rotation magnitudes of the SIC in the NE-lobe were quantified by unfolding the basal SIC contacts of the adjacent North Range (171/40) and East Range (264/70) portions as well as the respective primary remanence orientations in the SIC around the hinge line of the lobe (197/35: Klimczak et al. 2007). Specifically, the basal SIC contacts on either side of the hinge line were rotated until the contacts resulted in a common plane. Similarly, primary remanence directions of the North Range and the East Range SIC were rotated until their respective means were collinear. Unfolding of the basal SIC contact of the North Range and the East Range resulted in a common plane oriented at 230/40 (Fig. 3a). As the basal SIC contact segments in their present positions enclose an angle of 104°, the rotation magnitude after unfolding amounts to 76°.

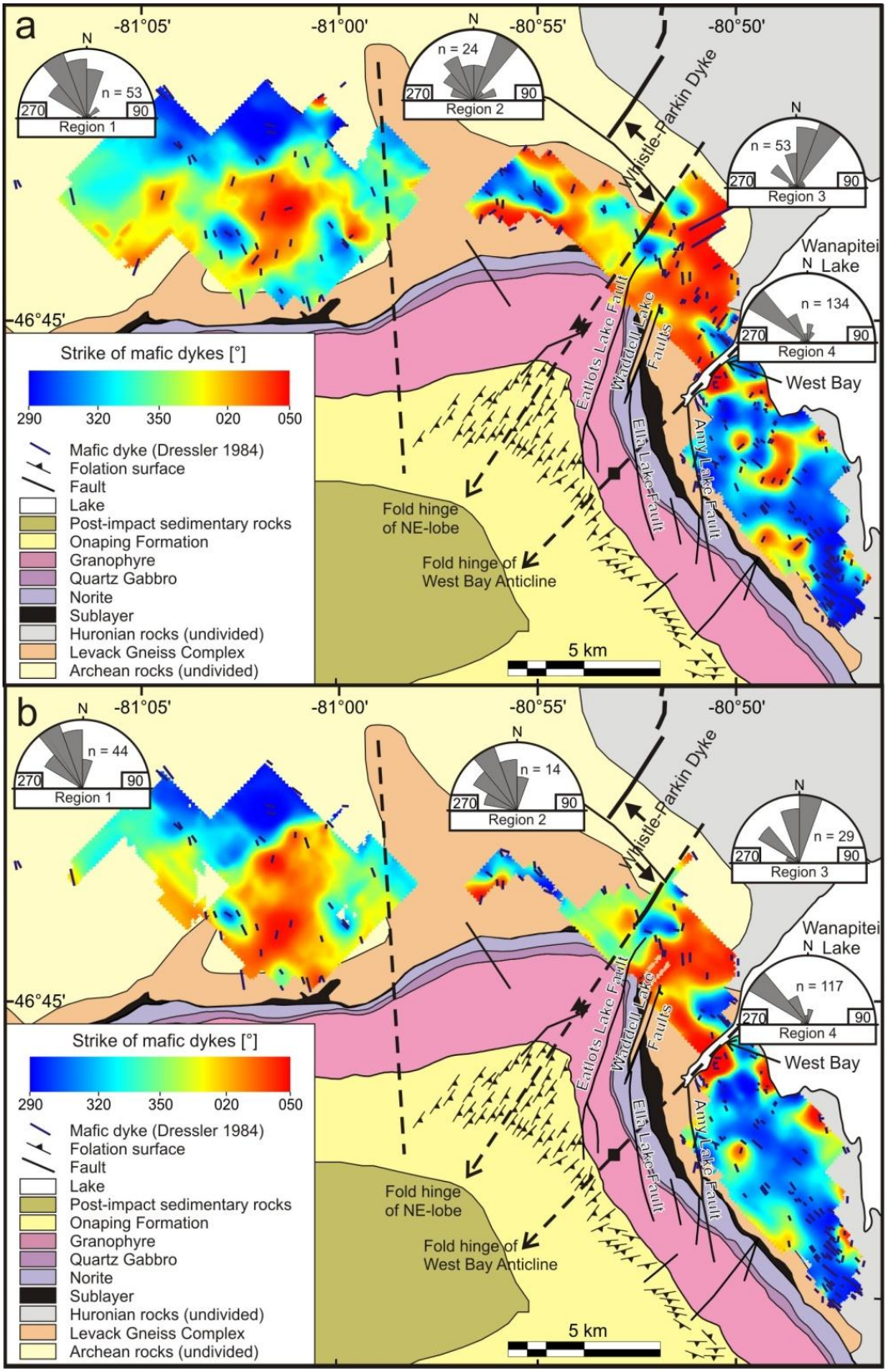
a
-81°05'
-81°00'
-80°55'
-80°50'
-46°45'
N
n = 53
Region 1
n = 24
Region 2
n = 53
Region 3
n = 134
Region 4
Whistle-Parkin Dyke
Wanapitei Lake
West Bay
Eatlots Lake Fault
Waddell Lake Faults
Ella Lake Fault
Anny Lake Fault
Fold hinge of NE-lobe
Fold hinge of West Bay Anticline
5 km
Strike of mafic dykes [°]
290 320 350 020 050
Mafic dyke (Dressler 1984)
Folation surface
Fault
Lake
Post-impact sedimentary rocks
Onaping Formation
Granophyre
Quartz Gabbro
Norite
Sublayer
Huronian rocks (undivided)
Levack Gneiss Complex
Archean rocks (undivided)
b
n = 44
Region 1
n = 14
Region 2
n = 29
Region 3
n = 117
Region 4

Figure 4: Geological maps of the northeastern Sudbury Basin showing interpolated surfaces of the strikes of mafic dykes in Archean rocks underlying the SIC. Color changes signify distinct zones at which overall dyke strikes change. Note such changes between regions 2 and 3, i.e., the northeastward continuation of the hinge line of the NE-lobe, and between regions 3 and 4, i.e., at the West Bay of Wanapitei Lake. (a) Interpolated surface of the strikes of all dykes. Radii of rose diagrams are the same as in Figure 2. (b) Interpolated surface of strike of dykes excluding NE-striking dykes. Radii of rose diagrams for regions 1 to 4 are respectively 14, 4, 10 and 58 dykes.

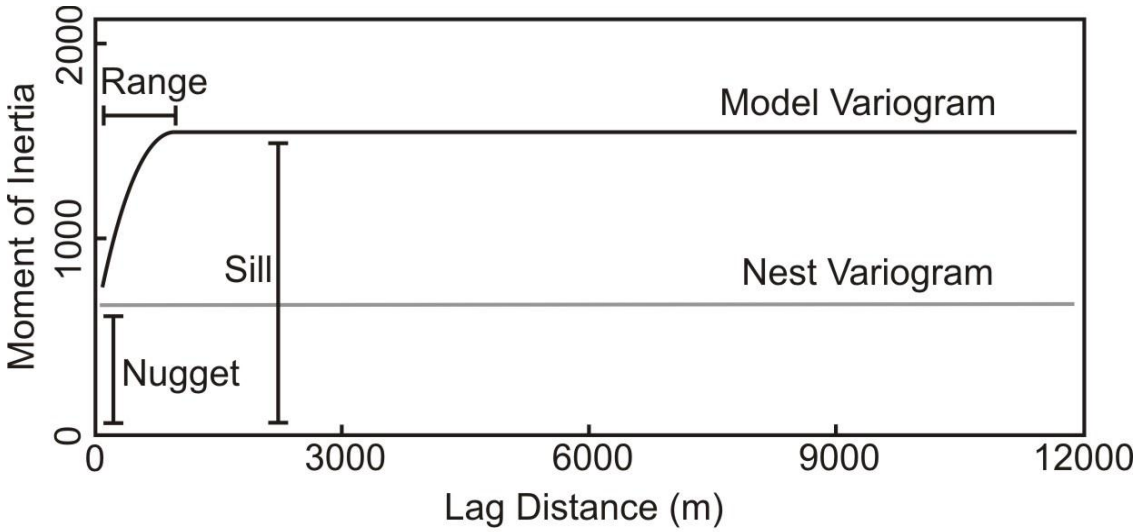

Figure 5: Variogram for the interpolated surfaces of dyke strikes shown in Figure 4. The variogram analysis indicates that a spherical model best represents the variogram of the strike of mafic dykes. The moment of inertia is the mean square difference between pairs of strike measurements from two sets of dykes. The lag distance represents distances of pairs of dykes and the curve of the spherical model is defined by the sill, the range and the nugget of the dyke data set. The sill represents the point at which strike-correlation between the dykes no longer exists. The range is defined as the distance (or lag) where two locations of dykes are no longer correlated. The nugget, which is also represented by the nest variogram, can indicate one or the combination of microscale variation and measurement error. My model variogram is defined by a direction of 335° with a range, nugget, and sill of 925.3m, 667.5m, and 876.5m, respectively. With a 50m cell size, this method used a search radius with 4 quadrants with its major axis oriented at 315° and a search distance of 1000m in both the major and minor directions. To achieve the grid-coverage in Figure 4, one search expansion and one grid pass was used. For further details on ordinary kriging, the reader is referred to Isaaks and Srivastava (1989) p. 278-322.

Primary magnetic remanence directions from the North Range SIC (n: 42) and the East Range SIC (n: 12) are scattered considerably (Figs. 1b, 3b). This is likely due to the shape change from a planar sheet geometry of the SIC into a segmented, inclined arc for

the case of the North Range (Morris 1984) and buckling of the eastern SIC into multiple higher-order folds in the East Range (Fig. 1b). In order to eliminate the influence of faulting and folding of the SIC on the scale larger than the NE-lobe, only remanence directions from the eastern North Range (n: 22) and from the northern East Range (n: 4) were used in the unfolding procedure. This resulted in well-defined clusters of remanence directions for the North Range and East Range SIC and respective mean remanence directions of 335/69 and 073/66 (Fig. 3c). Assuming that both limbs of the NE-lobe rotated equal magnitudes, unfolding of the lobe lead to a single pre-folding remanence direction oriented at 027/74 (Fig. 3c). The remanence-based magnitude of unfolding of the NE-lobe amounts to 36° and final orientations of the basal North Range and East Range SIC of 198/37 and 251/58, respectively (Fig. 3c).

Petrography of Mafic Dykes

To identify the swarm or swarms to which individual mafic dykes east of the SIC belong, the petrographic field characteristics and locations of dykes were recorded. Dykes in outcrop vary in thickness between a few to tens of meters. Large plagioclase phenocrysts set in a generally medium-grained, dark matrix of retrogressed, mafic minerals is a common characteristic of the dykes. Collectively, these characteristics fit the petrography of Matachewan dykes and possibly Biscotasing dykes (Halls and Palmer 1990, Halls et al. 2008). My recorded locations of the dykes (Fig. 2), almost all of which adhere to these petrographic characteristics, correspond to dyke occurrences originally mapped by Dressler (1982, 1984). Based on the spatial correlation and petrography, it appears most plausible to us that the majority of dykes in Archean rocks underlying the East Range are part of the Matachewan swarm, although some dykes, notably the NE-striking ones, may belong to the Biscotasing swarm.

Variation in Strike of Mafic Dykes

The strike of mafic dykes varies considerably in Archean basement rocks underlying the eastern North Range and East Range (Fig. 2). Based on visual inspection of dyke strikes, I divided the study area into four regions, each of which is characterized by distinct strikes of dykes (Fig. 2). In regions 1 and 2, dyke strikes cluster around NNW directions and approximate the strike of Matachewan dykes in unstrained terranes north of the Sudbury Basin (Ernst and Halls, 1984; West and Ernst, 1991). However, region 2 shows also a prominent cluster of NE-striking dykes. Region 3 hosts predominantly NE-striking dykes, whereas region 4 displays a distinct cluster of NW striking dykes, indicating significant differential rotations of basement rocks between these regions.

Interpolation of dyke strikes applying the kriging method defines more distinctly areas of preferred dyke strikes (Fig. 4). The interpolation shows two NE-trending zones, across which dyke orientations change noticeably. Interestingly, the bounds between these zones coincide spatially with major known structures. The northern zone boundary is congruent with the hinge line trace of the NE-lobe and the southern zone boundary coincides with the West Bay Lineament, evident by the straight contour of the north shore of Wanapitei Lake (Fig. 4a). Incidentally, these zones correspond respectively to the boundaries of regions 2 and 3 and regions 3 and 4.

As mentioned above, it is uncertain whether all mafic dykes in Archean rocks north and east of the SIC belong to a single swarm, i.e., the Matachewan swarm. In fact, in addition to NNW and NE directions all regions show clusters of variable magnitude of NE-striking dykes or dyke segments (Figs. 2, 4a) that may belong to the Biscotasing swarm. The possible presence of multiple dyke populations in all regions renders the identification of rotational components between individual regions based on dyke strike imprecise. To better accentuate rotational components I recalculated the dyke strike

interpolation surface with just one dyke population by selectively eliminating NE-striking dykes from the data base. This interpolation resulted in a more distinct dyke orientation for each region and in an even better defined boundary between regions 2 and 3, the hinge line of the NE-lobe, in particular (Fig. 4b).

In order to find out whether abrupt changes in dyke strike can be reconciled with folding, a N-S striking, vertical plane, representing the primary orientation of Matachewan dykes (Fig. 1b; Ernst and Halls, 1984; West and Ernst, 1991), was rotated around the fold axis of the NE-lobe (Fig. 6a). Specifically, the plane was rotated by 18° and 38°, adhering respectively to the paleomagnetically constrained rotation magnitude and the unfolding magnitude of the basal SIC contact for each limb. This resulted in NNW-SSE striking planes for the NW-limb and NNE-SSW striking planes for the SE-limb of the NE-lobe (Fig. 6a). The strikes of these planes are consistent with the overall strike of dykes in the eastern North Range, i.e., regions 1 and 2, and east of the NE-lobe's hinge zone, i.e., region 3 (Fig. 4b).

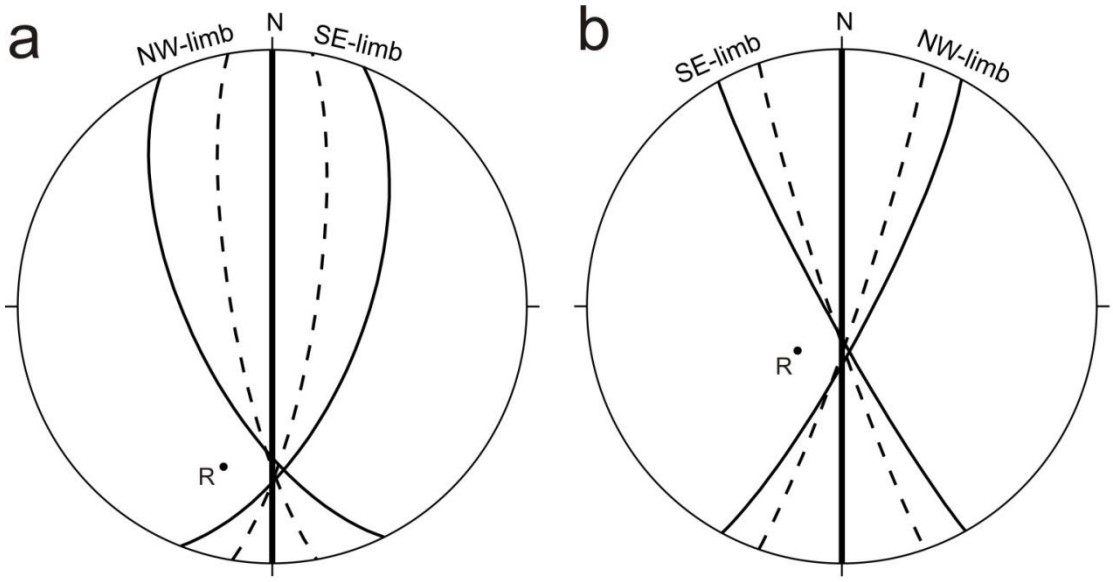

Figure 6: Diagrams showing the rotations of Matachewan dykes for the NE-lobe and the West Bay Anticline. (a) Folding of undeformed Matachewan dykes, represented by a subvertical N-S striking plane (bold great circle), around the hinge line R (197/35) of the NE-lobe by ±18° (stippled great circles) and ±38° (solid great circles). (b) Folding of undeformed Matachewan dykes, represented by a subvertical N-S striking plane (bold great circle), around the hinge line (R: 225/70) of the West Bay Anticline by ±20° (stippled great circles) and ±30° (solid great circles).

Similarly, the primary orientation of Matachewan dykes was used to test whether the West Bay Lineament constitutes the axial trace of a prominent fold. However, in contrast to the NE-lobe, magnitudes of limb rotations are not constrained paleomagnetically in this area. Judging, however, by the plan-view curvature and steep southwestward dip of the SIC (Dreuse et al. 2010), the East Range SIC forms an open anticline that plunges steeply toward the southwest. This amounts to limb rotations of 20° to 30° and a fold axis orientation of approximately 225/70. Respective rotations of planes representing primary dyke orientations resulted in NNW-SSE and NNE-SSW striking planes (Fig. 6b). The strikes of these planes match respectively with the strikes of dykes to the south (region 4) and north (region 3) of the lineament, (Figs. 4b). Thus, excluding NE-striking mafic dykes, the strikes of dykes in Archean rocks underlying the East Range are consistent with the possibility that the West Bay Lineament forms the hinge zone of a steeply southwest-plunging anticline, herein referred to as the West Bay Anticline, which affected Archean basement rocks.

2.6. Discussion

My analyses show that the variation in the strike of mafic dykes is consistent with tilting of Archean basement rocks around SW-plunging axes that affected the East Range SIC. Thus, tilting of basement rocks seems to have occurred mostly after the emplacement of the SIC and is attributed to the formation of the NE-lobe and the West Bay Anticline. The geometric compatibility of statistically preferred dyke strikes with rotation of the respective fold limbs (Figs. 4b, 6) indicates that impact-induced

deformation did not affect significantly the dyke orientations on the kilometer or larger scales. Anomalies of dyke strike on the hundred meter scale (Fig. 4) on the other hand may well be due to distortion of basement rocks as a result of cratering or pre-impact orogenic deformation.

Riller (2005) proposed that a west-plunging anticline, the hinge zone of which is located half way between the NE-lobe and the SE-lobe, caused the map-view curvature of the East Range SIC (Fig. 1b). This anticline is at variance with the position and plunge of the West Bay Anticline identified in this study. Based on the variation in the strikes of mafic dykes, map-view curvature of the SIC and geomorphic characteristics, i.e., the spatial correspondence of the hinge line trace with the West Bay Lineament, the West Bay Anticline accounts better for the structural characteristics of the East Range than the location of the fold axis previously suggested by Riller (2005).

The hinge line orientations of the West Bay Anticline and the NE-lobe depart significantly from the overall NNE-strike of planar structures of the Sudbury Basin (Fig. 1b). This departure may be due to localization of folding strain by a pre-existing structural anisotropy. Pre-impact planar mineral fabrics in Archean rocks underlying the northeastern SIC are weakly developed and random in orientation (Dressler 1984). Thus, such fabrics are unlikely to have caused the fold localization. Likewise, larger Archean or Paleoproterozoic fault zones predating the SIC are not known to have influenced the deformation of the SIC in the East Range. However, the base of the SIC in the NE-lobe is characterized by the Whistle embayment. Here, the Whistle-Parkin Offset Dyke protrudes northeastward, i.e., parallel to the hinge zone of the NE-lobe, into Archean gneiss and migmatite (Figs. 1, 2). As the Offset Dyke formed during cratering (Murphy and Spray 2002) or shortly after (Riller 2005, Hecht et al. 2008), it may well have served as a structural anisotropy that led to localization of post-impact folds in the basement rocks and the overlying SIC. Interestingly, the base of the SE-lobe is also characterized by a pronounced accumulation of Sublayer (Fig. 1b), from which the nearby Manchester dyke

may have been fed. It is, therefore, conceivable that Sublayer embayments and associated Offset Dykes served as zones of mechanical weaknesses, at which folding and faulting localized.

Norite and Sublayer are characterized by abrupt plan-view thickness variations in the hinge zone and limbs of the West Bay Anticline (Figs. 2, 4). The thickness variations are most conspicuous at the Waddell Lake Faults and the Amy Lake Fault (Fig. 4). The plan-view sinistral strike separations of lithologic contacts at these faults are kinematically consistent with NW-SE shortening that generated the West Bay Anticline. It should be noted that the Eatlots Lake, Waddell Lake, Ella Lake and Amy Lake Faults cannot be traced beyond the contact of the SIC with the Onaping Formation (Fig. 2). Folding strain in this Formation is accomplished by the pervasive development of metamorphic mineral fabrics (Cowan 1999; Cowan et al. 1999) that are axial-planar to the NE-lobe and the West Bay Anticline (Fig. 1b). Thus, discontinuous deformation in mechanically competent rocks such as the SIC and Archean basement rocks seems to have been transferred to continuous deformation in the mechanically less competent rocks of the Onaping Formation. The same deformational characteristics are known from rocks in the NE-lobe (Klimczak et al. 2007). The kinematics and curvature of the Eatlots Lake, Waddell Lake, Ella Lake and Amy Lake Faults and associated thickness variations in the lower SIC are consistent with folding strain imparted to the SIC and adjacent Archean rocks during formation of the West Bay Anticline.

Similar to the studies by Morris (1980b) and Szabó and Halls (2006), unfolding of the basal SIC contact around the SW-plunging axis of the NE-lobe did not result in a subhorizontal surface (Fig. 3a), as might be expected for an undeformed crater floor of this size. Back rotation of each limb amounts to 18°, based on primary paleomagnetic remanence directions (Fig. 3b), and 38° assuming a subhorizontal initial geometry of the basal SIC contact (Fig. 3a). At the time of remanence acquisition, the East Range basal

contact was, therefore, inclined moderately southwestward, whereas the eastern North Range basal contact was inclined moderately southward (Fig. 3a).

Two scenarios can account for the trough-like geometry of SIC basal contacts at the time of remanence acquisition. In the first scenario, rotation of the basal SIC contact by a maximum of 20° of each limb commenced prior to remanence acquisition. Assuming convective heat loss, the SIC solidified within about ten thousand years after impact (Prevec and Cawthorn 2002; Zieg and Marsh 2005), which approximates the time of remanence acquisition. This scenario requires unusually high, i.e., catastrophic, rotation (strain) rates to form the NE-lobe. Such a rather short period of folding appears inconsistent with the time required to form axial-planar metamorphic mineral fabrics in the Onaping Formation. Alternatively, much of the trough-like geometry of the SIC basal contact in the NE-lobe may be primary. This scenario appears more plausible, especially when considering the presence of the Whistle embayment in the hinge zone of the lobe. In this scenario, formation of the NE-lobe may have (1) localized at the embayment contacts, (2) led to tightening of these contacts by respectively 18° and (3) occurred at natural, i.e., non-catastrophic, geological strain rates.

Finally, it is noteworthy that the trace of the West Bay hinge zone, as inferred from the variation in strike of mafic dykes and SIC contacts, corresponds to prominent surface morphological characteristics, i.e., the straight NE-SW trending north shore of Wanapitei Lake and the West Bay Lineament. Photo lineaments in Precambrian shield regions are most commonly interpreted in terms of planar structures, such as faults and fracture zones which intersect the erosion surface, even though displacement of lithological contacts is not observed at the lineaments. My study suggests that photo lineaments in eroded basement terranes may be caused by linear structures, such as fold hinge zones, or the intersection of a fold-axial plane with the Earth's surface. These scenarios can account for the presence of lineaments, at which displacement of lithological contacts is not evident (cf. Drury 2001, p. 97).

2.7. Conclusions

Spatial analysis of the strike of mafic dykes is consistent with tilting of Archean basement rocks around SW-plunging axes that generated the NE-lobe and a newly identified anticline, the West Bay Anticline, in the East Range SIC. The hinge line trace of this anticline corresponds spatially to the known West Bay lineament. The West Bay Anticline accounts better for the structural characteristics of the East Range than a previously proposed anticline with west-plunging hinge line. The hinge zone and limbs of the West Bay Anticline is characterized by abrupt plan-view thickness variations in the lower SIC, which are most pronounced at the Waddell Lake and the Amy Lake Faults. The kinematics and curvature of these faults and the Eatlots Lake Fault as well as thickness variations in the lower SIC are consistent with folding strain imparted to the SIC and adjacent Archean rocks during formation of the West Bay Anticline. By contrast, folding strain in the mechanically less competent rocks of the overlying Onaping Formation was accomplished by continuous deformation.

Sublayer embayments and associated Offset Dykes served likely as zones of mechanical weaknesses, at which folds in the East Range localized. Unfolding magnitudes of the NE-lobe based on primary paleomagnetic remanence directions are significantly smaller than magnitudes based on the assumption that the basal SIC contact was initially planar. Thus, the basal SIC contact in the NE-lobe must have had a trough-like geometry at the time of remanence acquisition. I advocate a scenario for the formation of the NE-lobe, in which the trough geometry of the SIC is primary rather than a consequence of tilting prior to remanence acquisition of the SIC. In summary, my study shows that spatial analysis of planar markers, here mafic dykes, complemented by paleomagnetic data can help in recognizing folding strain in basement rocks at uppermost crustal levels. My study also suggests that photo lineaments in eroded basement terranes may be caused by linear structures, such as fold hinge zones, especially in cases where lithological contacts at lineaments are not displaced.

Chapter 3 – Plio-Pleistocene deformation on the Island of Rhodes, Greece, and its relationship to oblique subduction

3.1. Introduction

The mechanisms which control oblique subduction at curved subduction zone interfaces are not well known and their relative importance to subduction dynamics and observed fault pattern in the upper plate is still under question (Molnar and Tapponier, 1975). Specifically, the mechanisms which control subduction in the Mediterranean Sea have been of interest since their repeated impact on human development (Kontogianni et al. 2002, Shaw and Jackson 2010).

With recent advancements in marine geophysical surveys, seismic monitoring, and Global Positioning System (GPS) stations, a better understanding of the subduction zone mechanics in the Mediterranean region (Figure 7) has highlighted four dominant processes: (1) the westward extrusion of Anatolia into the Aegean (2) the southwestward plate motion of Aegean-Anatolia towards the Hellenic subduction zone, (3) rollback of the subducting African slab resulting in the southward migration of the Hellenic Arc, and (4) gravitational spreading in the Aegean (Dewey and Şengör 1979, Le Pichon and Angelier 1979, Le Pichon 1982, Taymaz et al. 1991, Gautier et al. 1999, Jolivet 2001). Although various hypotheses of the mechanisms which control the Hellenic subduction zone have been suggested, the relative importance of various proposed mechanisms is still in debate.

Addressing the relative importance of deformation processes associated with curved subduction zones requires a location where there is a strong obliquity between plate motion and the trace of the plate interface. Moreover, as the surficial expression of

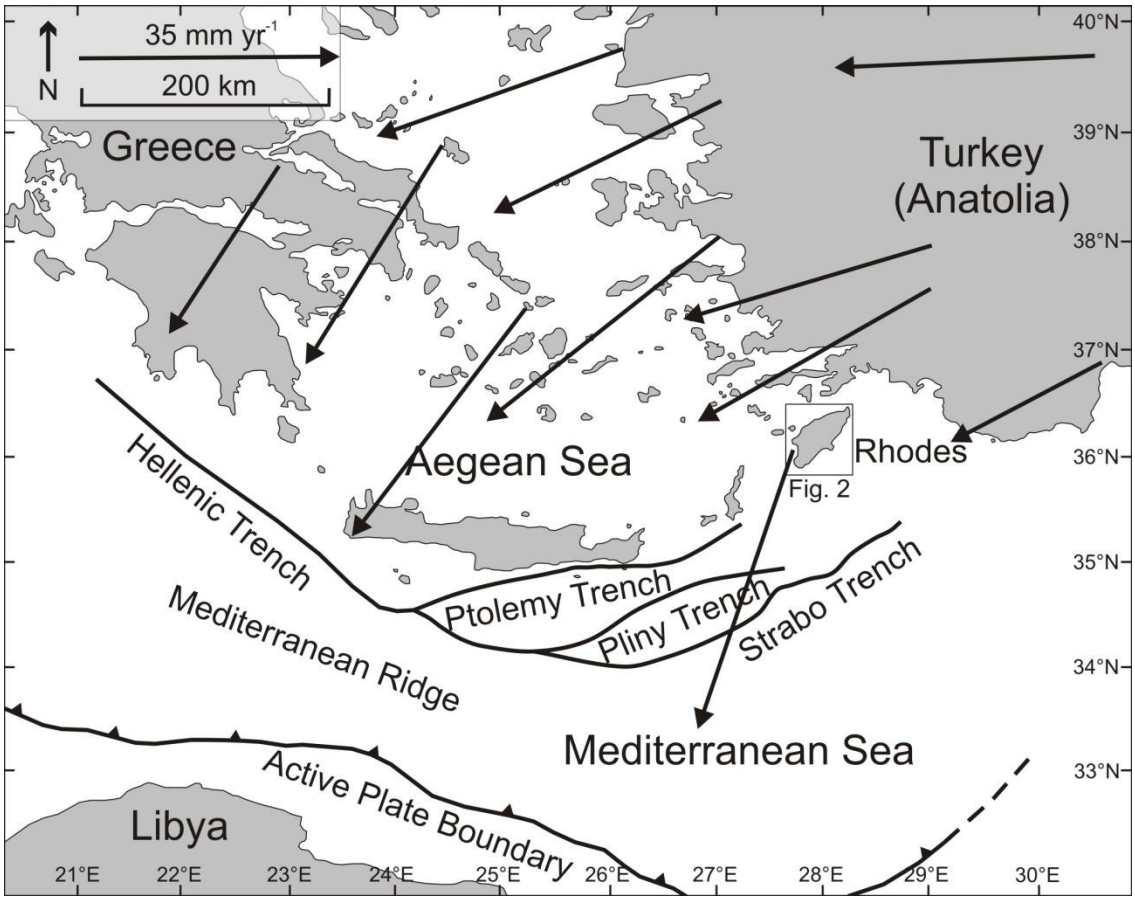

Figure 7: Geological overview of major eastern Mediterranean structures. Black arrows display GPS velocity vectors in respect to Eurasia after Reilinger et al. (2010). Vector magnitudes are on the order of 20-35 mm yr^{-1}.

the Hellenic Arc is submerged in the Mediterranean Sea, the opportunity to study upper-crust deformation is limited to only few exposures on islands such as Crete and Rhodes. The Island of Rhodes is located at the eastern end of the Hellenic arc and is ideally situated to be used to gauge the kinematics of upper-crustal deformation of the upper plate associated with oblique subduction.

Here, I address how upper-crustal rocks on the Island of Rhodes have been responding to ongoing oblique subduction since the late Miocene times. I present slip orientations and magnitudes for Pliocene to Recent faults on an island-wide scale based on the geological compilation map by Mutti et al. (1970). In addition, I use the slip orientations on individual faults to conduct a fault-slip analysis for the Island of Rhodes.

Finally, I present incremental horizontal strain ellipses for the island which I compare to regional faulting regimes.

3.2. Geological background information

Historically, there is account of various catastrophic events associated to ongoing plate subduction in the Mediterranean Sea. Examples include the 365 A.D. estimated 8.5+ magnitude earthquake on Crete resulting in a tsunami, which caused widespread destruction across the Mediterranean (Stiros 2010), and the 226 B.C. earthquake which collapsed the Colossus of Rhodes. This is due to the Hellenic Subduction Zone, a major lithospheric discontinuity found in the Eastern Mediterranean.

The Hellenic subduction zone is manifested by the collision of Africa and Aegea-Anatolia (Figure 7). The Aegean microplate (Aegea) is found underlying the Aegean Sea, bound by the Greek and Turkish mainland to the east and west. The Anatolian plate (Anatolia) lies to the east of Aegea and compromises the Turkish mainland. The African plate subducts northwards underneath Aegea at a rate of 35 mm yr^{-1}, which differs greatly from the rate of convergence between Africa and Eurasia of only 5-10mm yr^{-1} due to the southwestward motion of Aegea-Anatolia where both rates are relative to Eurasia (Figure 7) (McKenzie 1972, Reilinger et al. 2006). The difference in convergence rates has resulted in an increasing curvature of the Hellenic subduction zone since 11 Ma (ten Veen and Kleinsphen 2002). The westward component of plate motion is caused by the lateral extrusion of Anatolia into Aegea (McKenzie 1970, 1972). The southward plate motion of Aegea was diverted by Anatolia's lateral extrusion resulting in the present southwestward motion of Aegea. This has caused the Hellenic subduction zone to migrate southwestward associated with N-S upper plate extension in Aegea and slab rollback of the African Plate. In addition, gravitational spreading in Aegea has been identified as the mechanism which aids to accommodate horizontal crustal extension (Hatzfeld et al. 1997, Gautier et al. 1999).

The Hellenic subduction zone was thought to be a very young feature, 13 Ma (Le Pichon and Angelier, 1979), and 5 Ma (McKenzie 1978). It was not until seismic tomography studies indicated that the subducting African plate could be traced for a minimum length of 800 km, these estimates have been revisited for the onset of Hellenic subduction (Spakman et al. 1988, 1993, Bijwaard et al. 1998).

Currently, the only topographic expression of the Hellenic subduction zone is the Hellenic trench (Figure 7), where the plate interface found to the south is covered by accretionary sediments up to 1 km thick termed the Mediterranean Ridge (Figure 7, Le Pichon et al. 1982). The Hellenic Trench branches into 3 notable trenches east of Crete, the Ptolemy, Pliny, and Strabo trenches. These trenches display a sinistral strike-slip sense of movement (Le Pichon et al. 1995). The Hellenic Trench, more appropriately termed as a topographic scarp, is hypothesized to be generated by ongoing reverse faulting, essentially backstop faulting associated with subduction (Taymaz et al. 1990).

The Island of Rhodes resides along the eastern portion of the Hellenic Trench (Figure 7). It represents an uplifted segment of the Aegean upper crust as a heterogeneous assemblage of pre-Neogene Alpine nappes from the Mesozoic and Paleogene age and younger coastal sediments (Figure 8, Mutti et al. 1970). The Alpine nappes are strongly deformed, and occur as series of piled and folded lithotectonic units. Sediments infill basins between nappe stacks as non-marine clastic sequences of Mio-Pliocene age (Meulenkamp et al. 1972). During the Pliocene the Island of Rhodes was still a part of the Anatolian mainland, where more non-marine clastic sediments continued to infill the island basins. This was followed by a phase of block faulting during the late Pliocene and Pleistocene (Van Hinsbergen et al. 2007) and subsequent separation from Turkish mainland into the island seen today.

Of the sedimentary sequences, three sequences were deposited after the Late Miocene. The first sequence, known as the Levantian Formation, occurs as clastic sedimentary rocks (fluvial conglomerates and lacustrine grey marls) deposited during the late Miocene to early Pliocene. The second sequence, known as the Sgourou Formation,

occurs as coastal sedimentary rocks such as marls and coquinas deposited during the late Pliocene to Pleistocene. The third sequence, the Poros Formation, consists of coastal sedimentary rocks such as calcareous concretions formed during the Pleistocene.

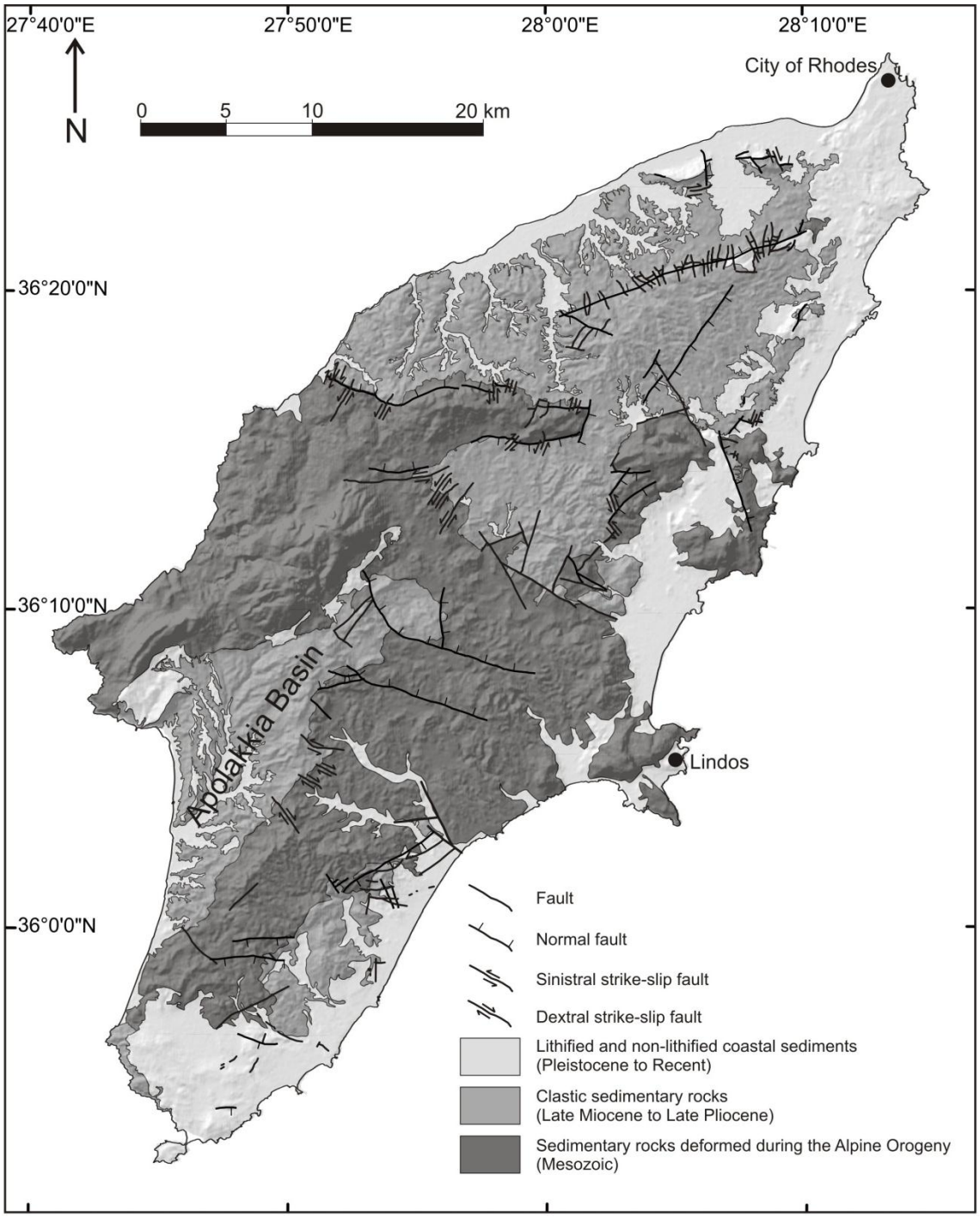

Figure 8: Geological overview of the Island of Rhodes. Faults which displace Late Miocene or younger formations are displayed. Topography displayed by 30m ASTER DEM with hillshading. Geological units compiled from Mutti et al. 1970.

3.3. Methods

Faults displacing Pliocene or more recent formations were compiled from the geological map of Rhodes generated by Mutti et al. (1970). To discern whether a given fault displaces Pliocene or more recent formations, faults in contact with the Levantian Formation, Sgourou Formation, and Poros Formation were analyzed for any evidence of displaced lithological boundaries or drastic elevation changes. The orientation and length of these faults were spatially analyzed. Using the elevation and location of Plio-Pleistocene displaced geologic units in contact with a fault and the three-point problem (Bennison et al. 2011), fault-slip vectors were calculated. Moreover, a fault-slip analysis was conducted to identify principal strain axis orientations, where axis orientations are calculated by the direct inversion analysis (Angelier 1990) and numerical dynamical analysis (NDA, Turner 1953, Spang 1972, Sperner et al. 1993) in the TectonicsFP software package (Ortner et al. 2002). I interpret the results of the fault-slip analysis in terms of strain instead of (paleo) stress due to origin of information being deformed rocks. Lastly, using the fault-slip vectors, horizontal strain ellipses were generated for the island using the software SPO2003 v.6 written by Launeau and Robin (2003).

3.4. Results

Based on inspection of the geological map (Mutti et al. 1970), 216 faults were identified to have been active since the beginning of the Pliocene identified from displaced Levantian or younger Formations (Figure 8). Many faults with normal sense of motion are crosscut by apparently younger faults showing strike-slip displacement components. Of these faults, slip vectors could be extracted from 67 faults, which

indicate that almost all faults contain components of normal and strike-slip motion and, therefore, should be termed oblique-normal faults. For this study, however, faults identified as oblique normal were grouped as either normal, or strike-slip due to the limitations of the fault slip routine. The magnitude of slip vectors were subsequently extracted from 27 faults (Figure 9).

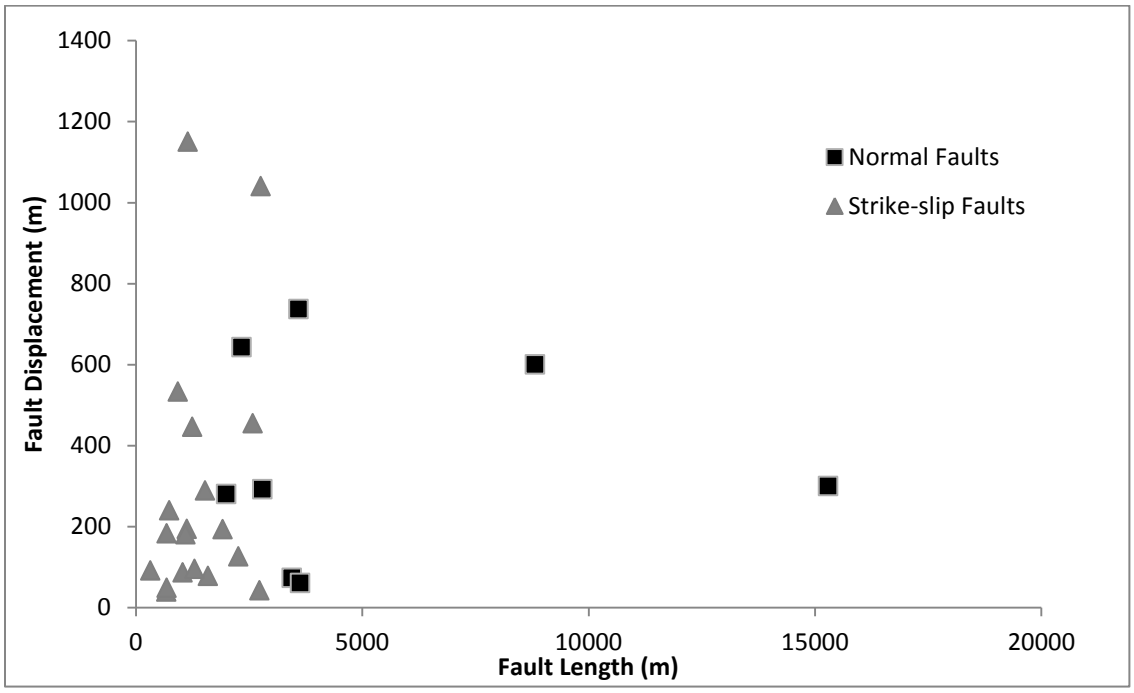

Figure 9: Scatter plot graph displaying the relationship between fault length and fault displacement. Fault length is defined as the length of the fault projected on the surface. Fault displacement is defined as the maximum slip length.

The fault-slip analysis was based on 67 faults where slip vectors were identifiable (Table 2). In addition to the cross-cutting nature of faults on the Island of Rhodes, the fault-slip analysis corroborated that there are two fault sets present, suggested by deviation in fault orientations shown by the so-called Angelier plot, and the lack of orthogonality between inferred principal strain axis orientations (Figure 10). Based on the Angelier plot, two fault sets are apparent. Set 1 consists of E-W striking normal faults and Set 2 is made up by predominantly NNE-SSW striking strike-slip faults. Based on

the assemblage of faulting on the Island of Rhodes, it is likely that there was initially a regime of horizontal extension, evident by normal faults, followed by a regime of horizontal shortening, seen by strike-slip faults cutting the normal faults.

Table 2: Fault orientations and magnitudes used for the fault-slip analysis. A slip magnitude value of 1 represents a fault where the slip magnitude could not reliably be determined.

ID	Dip Direction (°)	Dip (°)	Slip Azimuth (°)	Slip Plunge (°)	Slip Magnitude (m)
0	335.81	80	295	60	300
1	357.33	80	357.33	80	1
2	63.57	80	150	5	446
3	358.23	62	358.23	62	1
4	353.77	85	353.77	85	1
5	234.16	75	234.16	75	1
7	79.58	75	79.58	75	1
8	338.35	80	338.35	80	1
69	205.46	80	190	75	1
74	123.88	89	123.88	89	1
75	119.44	89	119.44	89	1
77	123.35	89	123.35	89	1
78	277.96	85	277.96	85	1
79	117.38	75	117.38	75	1
80	4.37	89	4.37	89	1
81	110.32	85	30	8	240
82	19.04	89	19.04	89	1
83	129.44	89	129.44	89	1
84	71.7	89	71.7	89	1
93	176.73	85	200	65	643
96	126.46	88	105	65	1
97	138.52	85	160	65	737
98	251.44	89	168	3	1150
99	231.42	89	145	3	533
111	105.86	85	105.86	85	1
112	164.92	80	164.62	80	1
113	95.55	70	15	9	87
114	178.51	80	178.51	80	1
115	132.13	89	210	3	181
116	175.23	75	200	60	1
117	4.11	85	10	81	1
119	357.68	80	357.68	80	1

120	351.68	85	270	3	1
121	126.53	86	40	3	126
122	132.16	80	48	3	193
123	122.68	89	37	3	1
125	287.1	86	10	3	49
126	1.34	85	5	81	1
132	105.23	87	190	3	183
133	86.81	89	1	3	194
134	16.76	75	16.76	75	1
135	30.33	65	30.33	65	1
136	271.72	80	271.72	80	1
137	20.69	85	20.69	85	600
138	346.11	85	346.11	85	292
139	186.45	80	186.45	80	280
141	18.98	80	300	5	1
145	11.71	80	11.71	80	1
146	343.78	75	343.78	75	1
147	119.15	89	35	3	78
148	7.68	80	7.68	80	1
149	28.89	85	28.89	85	1
150	36.39	85	36.39	85	1
151	15.56	85	15.56	85	1
152	28.01	85	28.01	85	1
153	7.77	85	7.77	85	1
154	109.93	89	15	3	91
155	15.89	89	15.89	89	1
156	118.39	89	30	3	42
157	120.31	89	205	3	39
158	26.64	89	115	1	95
159	30.1	89	118	3	289
192	175.78	85	160	75	1
194	191.7	85	191.7	85	1
208	177.09	68	155	50	1
214	55	89	135	3	455

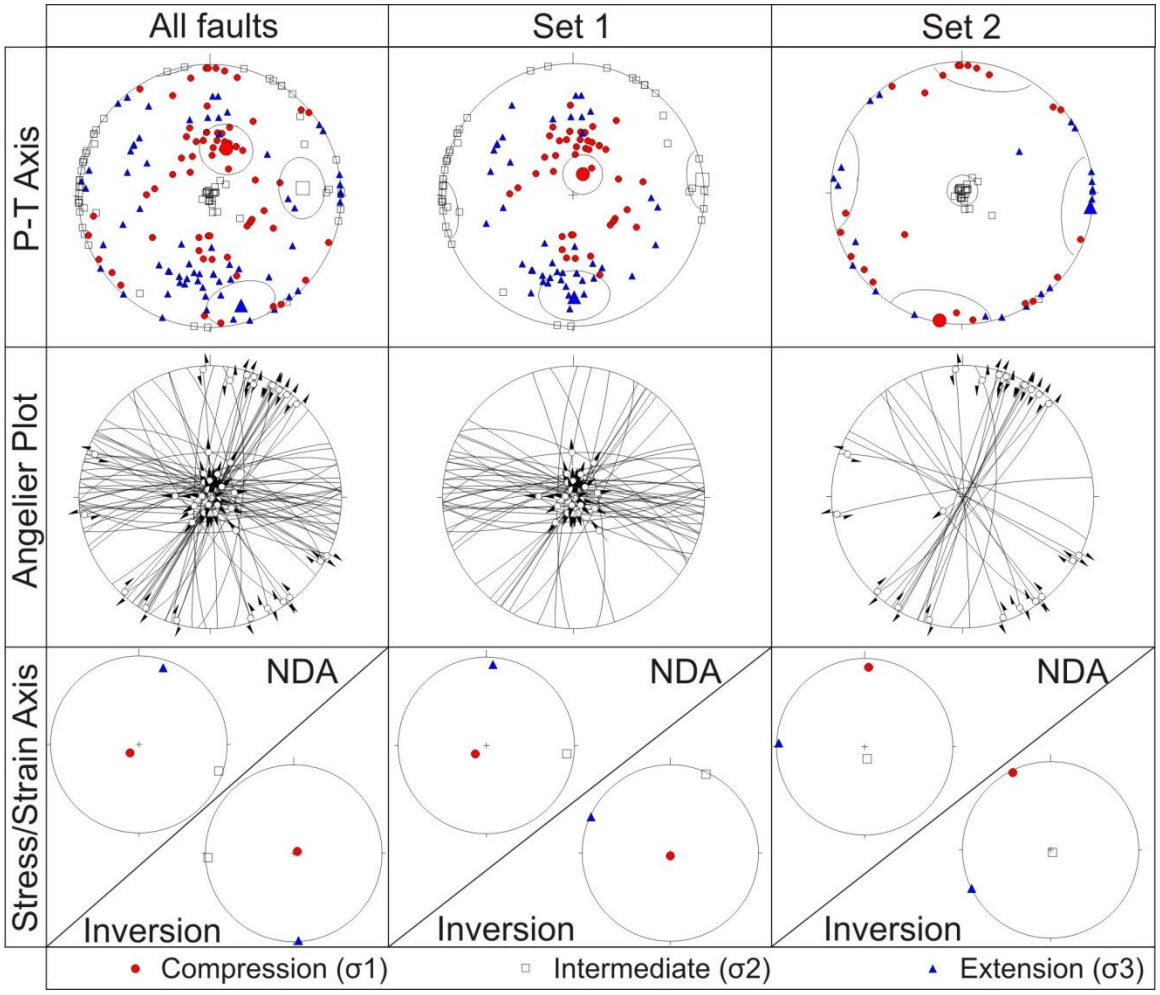

Figure 10: Fault-slip analysis results displayed in lower-hemisphere equal-area projections. P-T axis plots show the orientation of maximum and least principal compressive stresses. Angelier plot displays the orientation and sense of faults (Angelier and Goguel, 1979). NDA plot displays principal strain axes ($\hat{s}_1 > \hat{s}_2 > \hat{s}_3$). Inversion plot displays principal stress axes ($\sigma_1 > \sigma_2 > \sigma_3$). Set 1 faults correspond to the identified older normal faulting. Set 2 faults correspond to the identified younger strike-slip faulting.

Fault-slip analyses were conducted on each fault set. For Set 1 normal faults, the NDA and P-T methods indicate stress orientations where the maximum principal compressive stress (σ_1) is vertical and the maximum principal tensile stress (σ_3) is oriented N-S. This is similar to the stress axis orientations from the inversion method which indicate vertical shortening ($\hat{s}_3$) and NW-SE extension ($\hat{s}_1$). For Set 2 strike-slip

faults, the NDA and P-T methods indicate stress orientations where the maximum principal compressive stress (σ_1) is N-S and the maximum principal tensile stress (σ_3) is oriented E-W. This is similar to the stress axis orientations from the inversion method which indicate N-S shortening ($\hat{s}_3$) and E-W extension ($\hat{s}_1$).

The magnitude and orientation of slip vectors of the kilometer-scale faults were then used to calculate a horizontal finite strain ellipse (Figure 11a). As the data was separated into subsets on the basis of fault orientation, type, and visible cross cutting relationship, incremental strain ellipses were calculated for each subset (Figure 11b, c). The maximum diameter of the finite strain ellipse has an azimuth of 150° and a radius of 550m. The length of the radius of the minimum diameter amounts to 340m. Accordingly, the ellipticity is 1.615 (Figure 11a). The maximum diameter of the incremental strain ellipse calculated for the normal faults has an azimuth of 168° and a radius of 318m. The length of the minimum diameter amounts to 254m. Accordingly, the ellipticity of the incremental ellipse is 1.254 (Figure 11b). Lastly, the maximum diameter of the incremental strain ellipse calculated for the strike-slip faults has an azimuth of 149° with a radius of 580m. The length of the radius of the minimum diameter amounts to 342m. Accordingly, the ellipticity of the horizontal ellipse is 1.694 (Figure 11c).

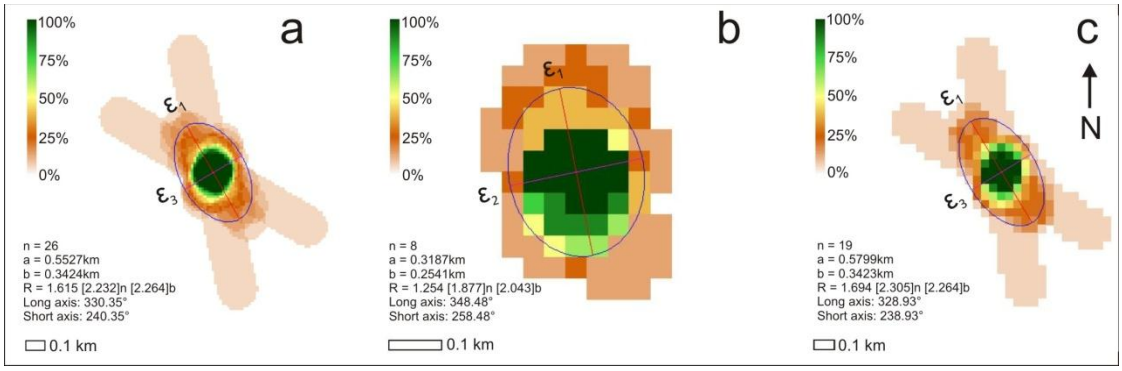

Figure 11: Strain ellipses generated from the horizontal component of fault-slip vectors using the SPO2003 v6 (a program for analyzing shape preferred orientation written by P. Launeau and P.F. Robin, 2012). n: number of faults, a: ellipse long axis, b: ellipse short axis, R: ellipticity. (a) Finite strain ellipse generated from all faults. (b) Incremental strain ellipse generated from Set 1 faults. (c) Incremental strain ellipse generated from Set 2 faults.

3.5. Discussion

Together, the variation in the strike and associated kinematics of faults in conjunction with the lack of orthogonality between calculated principal strain axes of the P-T plot suggests that there were multiple deformation regimes since the beginning of the Pliocene. During the first deformation regime, normal faulting was dominant with vertical shortening ($\hat{s}_3$) and NW-SE stretching ($\hat{s}_1$). This is in agreement with the suggested mechanisms of hinge rollback along the Hellenic Arc (Le Pichon and Angelier 1979, Le Pichon 1982) and gravitational spreading in the Aegean upper plate (Le Pichon et al. 1995, Jolivet 2001). As the subduction zone rolled back, the interface between the upper and lower plate migrated southward, causing the upper crust in the Aegean to thin. This resulted in widespread normal faulting with vertical shortening ($\hat{s}_3$) and N-S extension ($\hat{s}_1$) suggested by the fault-slip analysis and NNW-SSE extension ($\hat{s}_1$) suggested by the horizontal strain ellipse (Figure 10, 11b).

The second deformation regime is characterized by strike-slip tectonics in which the resulting principal strain orientations display N-S shortening ($\hat{s}_3$) and E-W extension ($\hat{s}_1$) suggested by the fault-slip analysis and NE-SW shortening ($\hat{s}_3$) and NW-SE extension ($\hat{s}_1$) suggested by the horizontal strain ellipse (Figure 10, 11c). Faults on the Island of Rhodes are found predominantly striking in two directions, E-W and NE-SW, which mimics the orientation of secondary faults known from simple shear deformation (Riedel 1929, Freund 1974). The mapped E-W faults manifest the strike-slip motion along the P-shear orientation and the NE-SW sinistral strike-slip faults manifest strike-slip motion along the R-shear orientation (Figure 12).

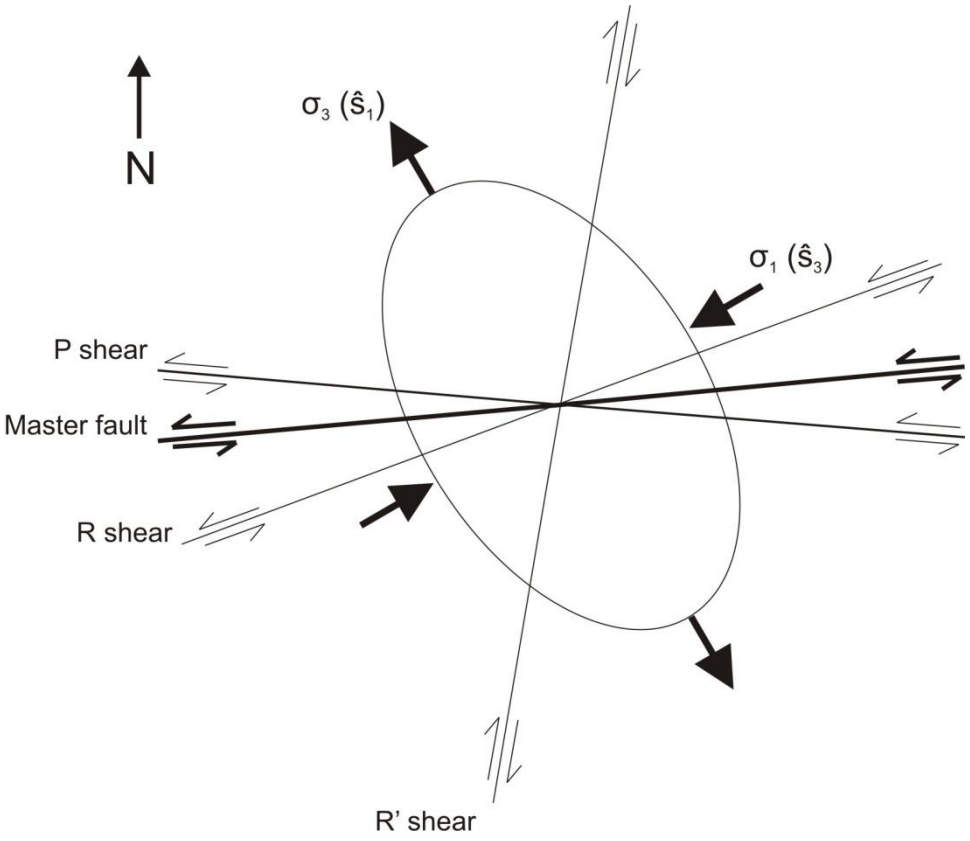

Figure 12: Model of shear fractures associated with simple shear with the incremental strain ellipse of Pliocene or younger deformation on the Island of Rhodes (shear model after Riedel 1929, Freund 1974). R shear: Riedel shear, R'-shear: Riedel prime shear, P-shear: pressure shear.

After the upper plate responded to hinge rollback with N-S extension and gravitational spreading, enhanced mechanical coupling between the upper and lower plates at their interface could result in the NE-SW striking sinistral strike-slip faults. As the upper plate thins during the first deformation regime, the enhanced friction between the thinned upper plate and subducting lower plate resulted in a stronger coupling. As subduction continued and the curvature of the Hellenic Arc increased (ten Veen and Kleinspehn 2002), areas along the Hellenic Arc with maximum obliquity in plate convergence experienced a change in the deformation regimes. The older N-S extension driven processes, namely, gravitational spreading and hinge roll-back changes as a result of increasing curvature of the Hellenic Arc. The increase in curvature of the Arc causes a

larger proportion of the Arc to subduct obliquely where mechanical coupling of the upper crust with the subducting crust becomes more influential to upper-crust deformation than the gravitational spreading/hinge roll back process associated with older N-S extensional tectonics. In the vicinity of the Island of Rhodes, this change in subduction dynamics resulted in principal strain orientations to change to N-S shortening ($\hat{s}_3$), E-W extension ($\hat{s}_1$). Due to this change in tectonic forces, the faulting regime on the Island of Rhodes shifted from normal faulting to strike-slip faulting. It is plausible that the strike-slip faults became active in conjunction with the onset of regional faults offshore such as the Pliny and Strabo trenches (Figure 7), both showing sinistral strike-slip motion (Le Pichon et al., 1995).

Ten Veen and Kleinspehn (2002) and this study recorded two kinematically distinct phases of deformation on the Island of Rhodes (Figure 7). The first kinematic phase is characterized by vertical shortening and N-S extension similar to the vertical shortening and NE-SW extension known from the Apolakkia Basin based on fault-slip analysis of small-scale shear faults (ten Veen and Kleinspehn, 2002). The second kinematic phase is characterized by N-S shortening and E-W extension which is similar to the oblique N-S shortening and oblique E-W extension from the Apolakkia Basin indicated by small-scale shear faults. When principal strain axes are compared to the orientation of distributed extension from Le Pichon and Kreemer (2010), principal strain axes from this study are closer in orientation to the regional distributed NW-SE extension than those from the Apolakkia Basin (Figure 13). This could be a result from deformation associated with the heterogeneity between the basin and the assemblage of Mesozoic basement rocks. As the fault-slip analysis of normal and strike-slip faulting is island-wide, it better relates to the regional kinematics of oblique subduction than fault-slip analyses based on small-scale shear faults conducted in a smaller area.

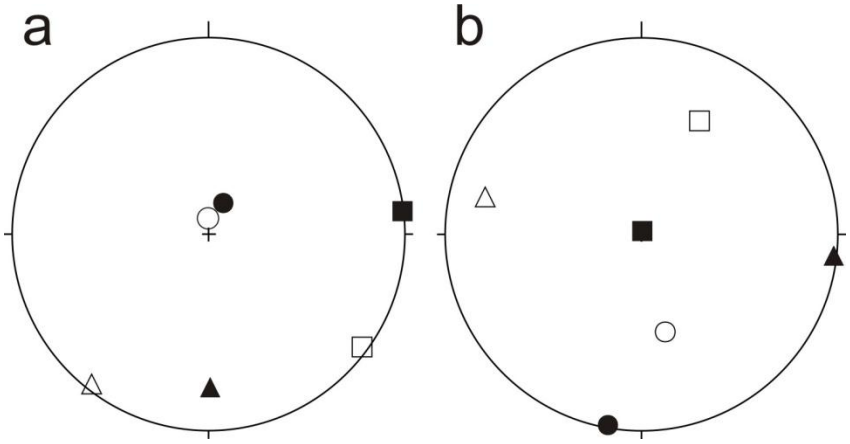

Figure 13: Comparison between the principal strain orientations from this study (black symbols) to those published from a local study of Apolakkia Basin (ten Veen and Kleinspehn, 2002, white symbols) displayed using lower-hemisphere equal-area projections. Triangles, squares, and circles represent shortening axes, the intermediate strain axes, and extension axes, respectively. (a) Principal strain orientations of Set 1normal faults. (b) Principal strain orientations of Set 2 strike-slip faults.

3.6. Conclusion

Kinematic analysis of kilometer-scale faults indicates that the Island of Rhodes has undergone two kinematically distinct deformation phases since the beginning of the Pliocene. The orientation of principal strain axes associated with older normal faulting is consistent with extensional N-S tectonics caused by gravitational spreading and hinge roll back of the Aegean Plate. The orientation of principal strain axes associated with the younger strike-slip faulting is consistent with a change in extensional tectonics to E-W extension and N-S shortening associated to an increase in mechanical coupling between the lower and upper plates.

References

Ames, D.E., Davidson, A., Buckle, J.L., and Card, K.D., 2005. Geology, Sudbury Bedrock Compilation. Geological Survey of Canada, Ontario, Open File 4570.

Angelier, J., 1990. Inversion of field data in fault tectonics to obtain the regional stress-III. A new rapid direct inversion method by analytical means. Geophysical Journal International, **103**: 363-376.

Angelier, J., and Goguel, J., 1979. Sur une method simple de détermination des axes principaux des contraintes pour une population de failles. Comptes rendus de l'Académie des sciences, Paris, **288**: 307-310.

Bennison, G.M., Olver, P.A., and Moseley, K.A., 2011. An Introduction to Geological Structures & Maps. 8th Ed; Hodder Education, London, England.

Bijwaard, H., Spakman, W., and Engdahl, E.R., 1998. Closing the gap between regional and global mantle tomography. Journal of Geophysical Research, **103**: 30055-30078.

Boast, M., and Spray, J.G., 2006. Superposition of a thrust-transfer fault system on a large impact structure: implications for Cu-Ni-PGE exploration at Sudbury. Economic Geology, **101**: 1583-1594.

Buchan, K.L., Mortensen, J.K., and Card, K.D., 1993. Northeast-trending Early Proterozoic Dykes of the southern Superior Province: multiple episodes of emplacement recognized fromintegrated paleomagnetism and U – Pb geochronology. Canadian Journal of Earth Science, **30**:1286-1296.

Chen, A., 1998. Geometric and kinematic evolution of basement-cored structures: intraplate orogenesis within the Yanshan Orogen, northern China. Tectonophysics, **292**: 17-42.

Choukroune, P., and Gapais, D., 1983. Strain pattern in the Aar Granite (Central Alps): Orthogneiss developed by bulk inhomogeneous flattening. Journal of Structural Geology, **5**: 411-418.

Coleman, A.P., 1907. The Sudbury Laccolithic Sheet. The Journal of Geology, **15**: 759-782.

Corfu, F., and Andrews, A.J., 1986. A U-Pb age for mineralized Nipissing diabase, Gowganda, Ontario. Canadian Journal of Earth Science, **23**: 107-109.

Cowan, E.J., 1999. Magnetic fabric constraints on the initial geometry of the Sudbury Igneous Complex: a folded sheet or a basin-shaped igneous body? Tectonophysics, **307**: 135-162.

Cowan, E.J., and Schwerdtner W.M., 1994. Fold origin in the Sudbury basin. *In* Proceedings of the Sudbury - Noril'sk Symposium *Edited by* Lightfoot, P.C. and Naldrett, A.J. Special Volume 5. Ontario Geological Survey, 45-55.

Cowan, E.J., Riller, U., and Schwerdtner, W.M., 1999. Emplacement geometry of the Sudbury Igneous Complex: Structural examination of a proposed impact melt-sheet. Geological Society of America Special Paper, **339**: 399-418.

Cristallini, E., Cominguez, A. H., and Ramos, V. A., 1997. Deep structure of the Metán-Guachipas Region: tectonic inversion in Northwestern Argentina. Journal of South American Earth Sciences, **10(5-6)**: 403-421.

Deutsch, A., Grieve, R.A.F., Avermann, M., Bischoff, L., Brockmeyer, P., Buhl, D., Lakomy, R., Müller-Mohr, V., Ostermann, M., and Stöffler, D., 1995. The Sudbury structure (Ontario, Canada): A tectonically deformed multi-ring impact basin. Geologische Rundschau, **84**: 697-709.

Dewey, J.F., and Sengör, A.M.C., 1979. Aegean and surrounding regions: complex multiplate and continuum tectonics in a convergent zone. Geological Society of America Bulletin, **90**: 84-92.

Dickin, A.P., Nguyen, T., and Crocket, J.D., 1999. Isotopic evidence for a single impact melting origin of the Sudbury Igneous Complex. *In* Large meteorite impacts and planetary evolution II. *Edited by* Dressler B. O. and Sharpton V. L. Geological Society of America Special Paper, **339**.

Dietz, R.S., 1964. Sudbury Structure as an Astrobleme. Journal of Geology, **72**: 412-434.

Dressler, B.O., 1982. Geology of the Wanapitei Lake Area, District of Sudbury; Ontario Geological Survey, Report 213, 131p. Accompanied by Maps 2450, 2451, scale 1:31 680 (l inch to '/2 mile).

Dressler, B.O., 1984. Sudbury Geological Compilation: Ontario Geological Survey Map 2491, Precambrian Geology Series, Scale 1:50 000.

Dreuse, R., Doman, D., Santimano, T., and Riller, U., 2010. Crater-floor topography and impact melt sheet geometry of the Sudbury impact structure, Canada. Terra Nova, **22**: 463-469.

Drury, S.A., 2001. Image interpretation in Geology. Nelson Thornes Ltd., Chaltenham, U.K.

Dudas, F.O., Davidson, A, and Bethune, K.M., 1994. Age of the Sudbury diabase dykes and their metamorphism in the Grenville Province, Ontario. Current Research, Geological Survey of Canada, **1994-F**: 97-106.

Ernst, R.E., and Halls, H.C., 1984. Paleomagnetism of the Hearst dike swarm and implications for the tectonic history of the Kapuskasing Structural Zone, northern Ontario. Canadian Journal of Earth Science, **21**: 1499-1506.

Erslev, E., 1986. Basement balancing of Rocky Mountain foreland uplifts. Geology, **14**: 259-262.

Fisher, R.A., 1953. Dispersion on a sphere. Proceedings of the Royal Society of London, **A217**: 295-305.

French, B.M., 1968. Sudbury structure, Ontario: some petrographic evidence for an origin by meteorite impact. Shock Metamorphism of Natural Materials: 383-412.

Freund, R., 1974. Kinematics of transform and transcurrent faults. Tectonophysics, **21** : 93-134.

Gapais, D., Bale, P., Choukroune, P., Cobbold, P.R., Mahjoub, Y., and Marquer, D., 1987. Bulk kinematics from shear zone patterns – some field examples. Journal of Structural Geology, **9**: 635-646.

Gautier, P., Brun, J.P., Moriceau, R., Sokoutis, D., Martinod, J., and Jolivet, L., 1999. Timing, kinematics and cause of Aegean extension: a scenario based on a comparison with simple analogue experiments. Tectonophysics, **315**: 31-72.

Grant R., W., and Bite, A., 1984. The Sudbury Quartz Diorite Offset Dikes. *In* The Geology and Ore deposits of the Sudbury Structure. *Edited by* Pye, E., Naldrett, A.J., and Giblin, P.E. Ontario Geological Survey Special Volume **1**: 275-300.

Grieve, R.A.F., Ames, D.E., Morgan, J.V., and Artemieva, N., 2010. The evolution of the Onaping Formation at the Sudbury Impact Structure. Meteoritics and Planetary Science, **45**: 759-782.

Grieve, R.A.F., Reimold, W.U., Morgan, J., Riller, U., and Pilkington, M., 2008. Observations and interpretations at Vredefort, Sudbury and Chicxulub: towards an empirical model of terrestrial impact basin formation. Meteoritics and Planetary Science, **43**: 855–882.

Grieve, R.A.F., Stöffler, D., and Deutsch, A., 1991. The Sudbury structure – controversial or misunderstood. Journal of Geophysical Research, **96**: 22753–22764.

Halls, H.C, and Shaw, E.G., 1988. Paleomagnetism and orientation of Precambrian dykes, eastern Lake Superior region, and their use for estimates of crustal tilting. Canadian Journal of Earth Science, **25**: 732-743.

Halls, H.C., 2009. A 100 km-long paleomagnetic traverse radial to the Sudbury Structure, Canada and its bearing on Proterozoic deformation and metamorphism of the surrounding basement. Tectonophysics, **474**: 493-506.

Halls, H.C., and Palmer, H.C., 1990. The tectonic relationship of two Early Proterozoic dyke swarms to the Kapuskasing Structural Zone: a paleomagnetic and petrographic study. Canadian Journal of Earth Science, **27**: 87-103.

Halls, H.C., Davis, D.W., Stott, G.M., Ernst, R.E., and Hamilton, M.A., 2008. The Paleoproterozoic Marathon Large Igneous Province: New evidence for a 2.1 Ga long-lived mantle plume event along the southern margin of the North American Superior Province. Precambrian Research, **162**: 327-353.

Hatzfeld, D., Martinod, J., Bastet, G., Gautier, P., 1997. An analog experiment for the Aegean to describe the contribution of gravitational potential energy. Journal of Geophysical Research, **102**: 649-659.

Heaman, L.M., 1997. Global mafic magmatism at 2.45 Ga: Remnants of an ancient large igneous province? Geology, **25**: 299–302.

Hecht, L., Wittek, A., Riller, U., Mohr, T., Schmitt, R.T., and Grieve, R.A.F., 2008. Differentiation and emplacement of the Worthington Offset Dike of the Sudbury Impact Structure, Ontario. Meteoritics and Planetary Sciences, **43**: 1659-1679.

Hood, P.J., 1961. Paleomagnetic Study of the Sudbury Basin. Journal of Geophysical Research, **66**: 1235-1241.

Isaaks, E.H., and Srivastava, R.M., 1989. An Introduction to Applied Geostatistics. Oxford University Press, New York, NY.

Jolivet, L., 2001. A comparison of geodetic and finite strain pattern in the Aegean, geodynamic implications. Earth and Planetary Science Letters, **187**: 95-104.

Jolivet, L., Faccenna, C., Huet, B., Labrousse, L., Le Pourhiet, L., Lacombe, O., Lecomte, E., Burov, E., Denèle, Y., Brun, J., Philippon, M., Paul, A., Salaün, G., Karabulut, H., Piromallo, C., Monié, P., Gueydan, F., Okay, A.I., Oberhänsli, R., Pourteau, A., Augier, R., Leslie, D., and Driussi, O., 2012. Aegean tectonics: Strain localization, slab tearing and trench retreat. Accepted 06/05/2012 for publication in Tectonophysics,

Keays, R.R., and Lightfoot, P.C., 2004. Formation of Ni-Cu-PGE sulphide mineralization in the Sudbury Impact Melt Sheet. Mineralogy and Petrology, **82**: 217–258.

Kley, J., Gangui, A. H., and Krüger, D., 1996. Basement-involved blind thrusting in the eastern Cordillera Oriental, southern Bolivia: Evidence from cross-sectional balancing, gravimetric and magnetotelluric data, Tectonophysics, **259**: 171-184.

Klimczak, C., Wittek, A., Doman, D., and Riller, U., 2007. Fold origin of the NE-lobe of the Sudbury Basin, Canada: Evidence from heterogeneous fabric development in the Onaping Formation and the Sudbury Igneous Complex. Journal of Structural Geology, **29**: 1744-1756.

Kontogianni, V.A., Tsoulos, N., and Stiros, S.C., 2002. Coastal uplift, earthquakes and active faulting of Rhodes Island (Aegean Arc): modeling based on geodetic inversion. Marine Geology, **186**: 299-317.

Krogh, T.E., Corfu, F., Davis, D.W., Dunning, G.R., Heaman, L.M., Kamo, S.L., Machado, N., Greenough, J.D., and Nakamura, E., 1987. Precise U-Pb isotopic ages of diabase dykes and mafic to ultramafic rocks using trace amounts of baddeleyite and zircon. In: Halls, H.C., Fahrig, W.F. (eds) Mafic Dyke Swarms. Geological Association of Canada Special Paper, **34**: 147-152.

Krogh, T.E., Davis, D.W., and Corfu, F., 1984. Precise U-Pb zircon and baddeleyite ages for the Sudbury area. *In* The geology and Ore deposits of the Sudbury Structure. *Edited by* Pye E., Naldrett, A.J., and Giblin, P.E. Ontario Geological Survey Special Volume **1**: 431-448.

Launeau, P., 2004. Mise en évidence des écoulements magmatiques par analyse d'images 2-D des distributions 3-D d'Orientations Préférentielles de Formes. Bulletin from the Geological Society of France, **175**: 331-350.

Launeau, P., and Cruden, A.R., 1998. Magmatic fabric mechanisms in a syenite: results of a combined anisotropy of magnetic susceptibility and image analysis study. Journal of Geophysical Research, Solid Earth, **103**: 5067-5089.

Launeau, P., and Robin, P., 1996. Fabric analysis using the intercept method. Tectonophysics **267**: 91-119.

Larochelle, A., 1969. Preliminary Results of a Study of the Paleomagnetism of the Sudbury Irruptive. Geological Survey of Canada Paper, **69**: 19-23.

Le Pichon, X., 1982. Land-locked basins and continental collision: the Eastern Mediterranean as a case example. *In* Mountain Building Processes. Academic Press, London: 201-211.

Le Pichon, X., and Angelier, J., 1979. The Hellenic arc and trench system: a key to the neotectonic evolution of the eastern Mediterranean area. Tectonophysics, **60** : 1-42.

Le Pichon, X., Chamot-Rooke, N., and Lallemant, S., 1995. Geodetic determination of the kinematics of central Greece with respect to Europe: Implications for eastern Mediterranean tectonics. Journal of Geophysical Research, **100**: 12675-12690.

Le Pichon, X., and Kreemer, C., 2010. The Miocene-to-Present Kinematic Evolution of the Eastern Mediterranean and Middle East and Its Implications for Dynamics. Annual Review of Earth and Planetary Sciences. **38**: 323-351.

Le Pichon, X., Lybéris, N., Angelier, J., and Renard, V., 1982. Strain distribution over the east Mediterranean Ridge: A synthesis incorporating new sea-beam data, Tectonophysics, **86**: 243-274.

Lenauer, I., and Riller, U., 2012. Geometric consequences of ductile fabric development from brittle shear faults in mafic melt sheets: Evidence from the Sudbury Igneous Complex, Canada. Journal of Structural Geology, **35**: 40-50.

Lightfoot, P.C., De Souza, H., and Doherty, W., 1993. Differentiation and source of the Nipissing Diabase intrusions, Ontario, Canada. Canadian Journal of Earth Sciences, **30**: 1123-1140.

McKenzie, D., 1970. Plate tectonics of the Mediterranean Region. Nature, **226**: 239-43.

McKenzie, D., 1972. Active tectonics of the Mediterranean Region, Geophysical Journal. Royal Astronomical Society, **30**: 109-185.

McKenzie, D., 1978. Active tectonics of the Alpine-Himalayan belt: the Aegean Sea and surrounding regions. Geophysical Journal. Royal Astronomical Society, **55**: 217-254.

Meulenkamp, J.E., De Mulder, E.F.J., and Van De Weerd, A., 1972. Sedimentary history and paleogeography of the Late Cenozoic of the island of Rhodos. Zeitschrift der Deutschen Geologischen Gesellschaft, **123**: 541-553.

Molnar, P., and Tapponier, P., 1975. Cenozoic tectonics of Asia. Science, **189**: 419-426.

Morris, W.A., 1980a. A positive fold test from Nipissing diabase. Canadian Journal of Earth Science, **18**: 591-598.

Morris, W.A., 1980b. Tectonic and Metamorphic History of the Sudbury Norite: The Evidence from Paleomagnetism. Economic Geology, **76**: 260-277.

Morris, W.A., 1981. Intrusive and Tectonic History of the Sudbury Micropegmatite: The Evidence from Paleomagnetism. Economic Geology, **76**: 791-804.

Morris, W.A., 1982. A Paleomagnetic Investigation of the Sudbury Basin Offsets, Ontario, Canada. Tectonophysics, **85**: 291-312.

Morris, W.A., 1984. Paleomagnetic Constraints on the Magmatic, Tectonic, and Metamorphic History of the Sudbury Basin Region. *In* The Geology and Ore deposits of the Sudbury Structure. *Edited by* Pye, E., Naldrett, A.J., and Giblin, P.E. Ontario Geological Survey Special Volume **1**: 411-427.

Morris, W.A., and Pay, R., 1981. Genesis of the Foy (?) Offset and Its Sulfide Ores: The Paleomagnetic Evidence from a Study in Hess Township, Sudbury, Ontario. Economic Geology, **76**: 1895-1905.

Morrison, G.G., 1984. Morphological features of the Sudbury structure in relation to an impact origin. *In* The geology and ore deposits of the Sudbury structure. *Edited* by Pye, E., Naldrett, A.J., Giblin, P.E. Ontario Geological Survey Special Volume **1**: 513-522.

Murphy, A.J., and Spray, J.G., 2002. Geology, Mineralization, and Emplacement of the Whistle-Parkin Offset Dyke, Sudbury. Economic Geology, **97**(7): 1399-1418.

Mutti, E., Orombelli, G., and Pozzi, R., 1970. Geological studies on the Dodecanese islands (Aegean Sea). IX. Geological map of the island of Rhodes (Greece). Explanatory notes. Annuaire Géologique de Pays Hellénique, **22** : 77-226.

Nyst, M., and Thatcher, W., 2004. New constraints on the active deformation of the Aegean. Journal of Geophysical Research, **109**: B11406.

Ortner, H., Reiter, F., and Arc, P., 2002. Easy handling of tectonic data: the programs TectonicVB for Mac and Tectonics FP for Windows™. Computers & Geosciences, **28**: 1193-1200.

Pattison, E.F., 1979. The Sudbury Sublayer. Canadian Mineralogist, **17**: 257-274.

Pentek, A., Molnar, F., Watkinson, D.H., Jones, P.C., and Mogessie, A., 2011. Partial melting and melt segregation in footwall units within the contact aureole of the Sudbury Igneous Complex (North and East Ranges, Sudbury structure), with implications for their relationship to footwall Cu-Ni-PGE mineralization.

International Geology Review, **53**: 291-325.

Phinney, W.C., and Halls, H.C., 2001. Petrogenesis of the Early Proterozoic Matachewan dyke swarm, Canada, and implications for magma emplacement and subsequent deformation. Canadian Journal of Earth Science, **38**: 1541-1563.

Pope, K.O., Kieffer, S.W., and Ames, D.E., 2004. Empirical and theoretical comparisons of Chicxulub and Sudbury impact structures. Meteoritics and Planetary Science, **39**: 97-116.

Prevec, S.A., and Cawthorn, R.G., 2002. Thermal evolution and interaction between impact melt sheet and footwall: A genetic model for the contact sublayer of the Sudbury Igneous Complex, Canada. Journal of Geophysical Research-Solid Earth, **107**(B8): 2176.

Reilinger, R., McClusky, S.C., Vernant, P., Lawrence, S., Ergintav, S., Cakmak, R., Ozener, H., Kadirov, F., Guliev, I., Stepanyan, R., Nadariya, M., Hahubia, G., Mahmoud, S., Sakr, K., ArRajehi, A., Paradissis, D., Al-Aydrus, A., Prilepin, M., Guseva, T., Evren, E., Dmitrotsa, A., Filikov, S.V., Gomez, F., Al-Ghazzi, R., and Karam, G., 2006. GPS constraints on continental deformation in the Africa-Arabia-Eurasia continental collisional zone and implication for the dynamics of plate interactions, Journal of Geophysical Research, **111**: 1-26.

Riedel, W., 1929. Zur Mechanik geologischer Brucherscheinungen. Centralbl. F. Mineral. Geol. U. Pal., **1929B**: 354-368.

Riller, U., 2005. Structural characteristics of the Sudbury impact structure, Canada: Impact-induced versus orogenic deformation – A review. Meteoritics and Planetary Science, **40**: 1723-1740.

Riller, U., Cruden, A. R., and Schwerdtner, W. M., 1996. Magnetic fabric, microstructure and high-temperature metamorphic overprint of the Murray granite pluton, central Ontario. Journal of Structural Geology, **18**: 1005-1016.

Riller, U., Schwerdtner, W.M., and Robin, P.Y.F., 1998. Low-temperature deformation mechanisms at a lithotectonic interface near the Sudbury Basin, Eastern Penokean Orogen, Canada. Tectonophysics, **287**: 59-75.

Rousell, D.H., 1984. Structural Geology of the Sudbury Basin. *In* The Geology and Ore Deposits of the Sudbury Structure. *Edited by* Pye E.G., Naldrett A.J., and Giblin P.E. Ontario Geological Survey Special Publication **1**: 83-96.

Rousell, D.H., 1975. Origin of foliation and lineation in Onaping formation and deformation of the Sudbury Basin. Canadian Journal of Earth Science, **12**: 1379-1395.

Shanks, W.S., and Schwerdtner, W.M., 1991. Structural analysis of the central and southwestern Sudbury Structure, Southern Province, Canadian Shield. Canadian Journal of Earth Science, **28**, 411-430.

Shellnutt, J.G., and MacRae, N.D., 2012. Petrogenesis of the Mesoproterozoic (1.23 Ga) Sudbury dyke swarm and its questionable relationship to plate separation. International Journal of Earth Science, **101**: 3-23.

Sopher, S.R., 1963. Paleomagnetism study of the Sudbury Irruptive. Geological Survey of Canada, **90**: 1-34.

Spakman, W., Wortel, M.J.R., and Vlaar, N.J., 1988. The Hellenic subduction zone: a tomographic image and its geodynamic implications. Geophysical Research Letters, **15**: 60-63.

Spang, J.H., 1972. Numerical method for dynamic analysis of calcite twin lamellae. Geological Society of America Bulletin, **83**: 467-472.

Sperner, B., Ratschbacher, L., and Ott, R., 1993. Fault-striae analysis: a Turbo pascal program for graphical presentation and reduced stress tensor calculation. Computers & Geosciences, **19**: 1361-1388.

Spray, J.G., Butler, H.R., and Thompson, L.M., 2004. Tectonic influences on the morphology of the Sudbury impact structure: Implications for terrestrial cratering and modeling. Meteoritics and Planetary Science, **39**: 287-301.

Stiros, S.C., 2010. The 8.5+ magnitude, AD365 earthquake in Crete: Coastal uplift, topography changes, archaeological and historical signature. Quaternary International, **216**: 54-63.

Szabo, E., and Halls, H.C., 2006. Deformation of the Sudbury Structure: Paleomagnetic evidence from the Sudbury breccias. Precambrian Research, **150**: 27-48.

Taymaz, T., Jackson, J., and McKenzie, D., 1991. Active tectonics of the north central Aegean Sea. Geophysical Journal International, **106**: 433-490.

Taymaz, T., Jackson, J., and Westaway, R., 1990. Earthquake mechanisms in the Hellenic Trench near Crete. Geophysical Journal International, **102**: 695-731.

Ten Veen, J.H., and Kleinspehn, K.L., 2002. Geodynamics along an increasingly curved convergent plate margin: Late Miocene-Pleistocene Rhodes, Greece. Tectonics, **21**: 1-21.

Therriault, A.M., Fowler, A.D., and Grieve, R.A.F., 2002. The Sudbury Igneous Complex: A differentiated impact-melt sheet. Economic Geology, **97**: 1521-1540.

Tschirhart, P., Morris, W.A., 2012. Grenville age deformation of the Sudbury impact structure: evidence from magnetic modelling of the Sudbury diabase dyke swarm. Terra Nova, in press.

Turner, F.J., 1953. Nature and dynamic interpretation of deformation lamellae in Calcite of three marbles. American Journal of Science, **251**: 276-298.

Van Hinsbergen, D.J.J., Krijgsman, W., Langereis, C.G., Cornée, J., Duermeijer, C.E., and Van Vugt, N., 2007. Discrete Plio-Pleistocene phases of tilting and counterclockwise rotation in the southeastern Aegean arc (Rhodes, Greece): early

Pliocene formation of the south Aegean left-lateral strike-slip system. Journal of the Geological Society of London, **164**: 1133-1144.

West, G. and Ernst R., 1991: Evidence from aeromagnetics on the configuration of Matachewan dykes and the tectonic evolution of the Kapuskasing Structural Zone, Ontario, Canada. Canadian Journal of Earth Science, **28**: 1797-1811.

Wilson, H.D.B., 1956. Structure of Lopoliths. Geological Society of America, **67**: 289-300.

Zieg, M.J., and Marsh, B.D., 2005, The Sudbury Igneous Complex: viscous emulsion differentiation of a superheated impact melt sheet: Geological Society of America Bulletin, **117**: 1427–1450.